RSC Advances

REVIEW

View Article Online
View Journal | View Issue

Cite this: *RSC Adv.*, 2021, **11**, 31098

Expanding the PET radioisotope universe utilizing solid targets on small medical cyclotrons

K. J. H. George,[ab] S. Borjian,[e] M. C. Cross,[e] J. W. Hicks,[ab] P. Schaffer[defg] and M. S. Kovacs *[abc]

Received 9th June 2021
Accepted 25th August 2021

DOI: 10.1039/d1ra04480j

rsc.li/rsc-advances

Molecular imaging with medical radioisotopes enables the minimally-invasive monitoring of aberrant biochemical, cellular and tissue-level processes in living subjects. The approach requires the administration of radiotracers composed of radioisotopes attached to bioactive molecules, the pairing of which considers several aspects of the radioisotope in addition to the biological behavior of the targeting molecule to which it is attached. With the advent of modern cellular and biochemical techniques, there has been a virtual explosion in potential disease recognition antigens as well as targeting moieties, which has subsequently opened new applications for a host of emerging radioisotopes with well-matched properties. Additionally, the global radioisotope production landscape has changed rapidly, with reactor-based production and its long-defined, large-scale centralized manufacturing and distribution paradigm shifting to include the manufacture and distribution of many radioisotopes *via* a worldwide fleet of cyclotrons now in operation. Cyclotron-based radioisotope production has become more prevalent given the commercial availability of instruments, coupled with the introduction of new target hardware, process automation and target manufacturing methods. These advances enable sustained, higher-power irradiation of solid targets that allow hospital-based

[a]*Lawson Health Research Institute, 268 Grosvenor Street, London, ON, N6A 4V2, Canada. E-mail: mkovacs@lawsonimaging.ca*

[b]*Medical Biophysics, Western University, 1151 Richmond Street N., London, ON, N6A 5C1, Canada*

[c]*Medical Imaging, Western University, 1151 Richmond Street N., London, ON, N6A 5C1, Canada*

[d]*Life Sciences, TRIUMF, 4004 Wesbrook Mall, Vancouver, BC, V6T 2A3, Canada*

[e]*ARTMS, 301-4475 Wayburn Drive, Burnaby, BC, V5G 4X4, Canada*

[f]*Radiology, University of British Columbia, 2775 Laurel St, Vancouver, BC, V5Z 1M9, Canada*

[g]*Chemistry, Simon Fraser University, 8888 University Dr, Burnaby, BC, V5A 1S6, Canada*

Keller Joshell Hadassah George obtained her BSc in chemical engineering at the Illinois Institute of Technology in 2013. She then obtained her MESc and PhD at Western University in 2015 and 2019 respectively. She currently holds a Mitacs Accelerate Postdoctoral Fellowship at Western University/ARTMS, and her research focuses on the optimization of separation methods for cyclotron-produced ^{68}Ga on solid targets.

Sogol Borjian received a BSc (2005) and MSc (2007) in Polymer Engineering from Amirkabir University of Technology in Tehran, Iran. She then received a PhD (2014) in Organometallic Chemistry from Queen's University in Kingston, ON, where her research focused on developing new palladium catalysts for pharmaceutical applications. She followed with an Industrial Postdoctoral Fellowship in collaboration with ABB (Zurich) where her research focused on developing novel thin films for selective chemical sensing using micro-optical devices. Sogol joined ARTMS Inc. in 2018 and is currently responsible for managing the Chemistry and Target Production teams, overseeing the development and commercialization of medical radioisotopes used in cancer diagnosis and treatment.

radiopharmacies to produce a suite of radioisotopes that drive research, clinical trials, and ultimately clinical care. Over the years, several different radioisotopes have been investigated and/or selected for radiolabeling due to favorable decay characteristics (*i.e.* a suitable half-life, high probability of positron decay, *etc.*), well-elucidated chemistry, and a feasible production framework. However, longer-lived radioisotopes have surged in popularity given recent regulatory approvals and incorporation of radiopharmaceuticals into patient management within the medical community. This review focuses on the applications, nuclear properties, and production and purification methods for some of the most frequently used/emerging positron-emitting, solid-target-produced radioisotopes that can be manufactured using small-to-medium size cyclotrons (≤24 MeV).

Introduction

Positron Emission Tomography (PET) is one of several diagnostic imaging tools used to non-invasively assess metabolic activity in body tissue. PET scanning is sensitive enough to quantify changes in biological processes, making it an ideal candidate for assessing the efficacy of an early treatment plan or newly developed drugs.[1] PET makes use of radiotracers which permit the visual isolation of metabolic processes within

Michael Cross is a co-founder and COO of ARTMS Inc. where he is responsible for overseeing operational activities, establishing regulatory and clinical strategies, and innovator and research collaborations. Previously Michael was General Manager at the Centre for Probe Development and Commercialization (McMaster University). Michael has over 20 years of healthcare and life science industry experience. Michael co-founded and was COO/CBO of OncoSec Medical and was also the SVP and co-lead of a $330 M life sciences venture fund. Michael received his PhD in physiology and MBA from the University of Toronto and was a post-doctoral fellow with the Department of National Defence.

Paul Schaffer obtained his PhD (Chemistry) in 2003 from McMaster University, after which he transitioned to become a Research Associate at McMaster Nuclear Reactor. This was followed by a role of Lead Scientist at GE Global Research. Since 2009, he has served as Associate Laboratory Director, Life Sciences at TRIUMF since 2012. Dr Schaffer is an Associate Professor in Radiology at the University of British Columbia, an adjunct professor in Chemistry at Simon Fraser University and is affiliated with the Research Center for Nuclear Physics at Osaka University. Dr Schaffer now serves as Chief Technology of ARTMS, Inc.; a spin-off company resulting from his research in large-scale cyclotron-based production of ^{99m}Tc in response to the 2007–2009 supply crises.

Justin Hicks is a research scientist focusing on radiochemistry for molecular imaging applications to investigate pressing biomedical questions. He received a MSc in ^{99m}Tc chemistry under Dr John Valliant at McMaster University (2010). He then completed a PhD on PET tracer development with Drs Alan Wilson and Neil Vasdev at the University of Toronto (2015). Dr Hicks then joined the Lawson Health Research Institute cyclotron as a radiochemist to translate clinical PERS, followed in 2016 by appointments as a Lawson Scientist and Assistant Professor in Medical Biophysics at Western University.

Michael Kovacs received his PhD (Medicinal Inorganic Chemistry) from the University of British Columbia in 2001. Under an NSERC Industrial Fellowship, he worked at Advanced Cyclotron Systems Inc (ACSI) where he lead research and development work on automated radiochemistry synthesis and cyclotron targetry. He was recruited as a Scientist by the Lawson Health Research Institute in 2003 to create a PET cyclotron and radiochemistry research program (founded 2010). Dr Kovacs is currently the Director of the Lawson Cyclotron and is Assistant Professor in Medical Imaging and Medical Biophysics at Western University. His research interests include the production and application of metal ions to PET imaging.

specific tissues and cells. These radiotracers are composed of a radioisotope attached to a bioactive molecule (*e.g.* a small molecule, peptide, antibody, *etc.*), as demonstrated in Fig. 1. The choice of bioactive targeting molecule mainly depends on the process to be visualized but also on the molecule's ability to incorporate the radioisotope into the chemical structure of the pharmaceutical compound. However, choosing the radioisotope requires consideration of biocompatibility in addition to the assessment of physical and biological half-life suitability for the metabolic process under investigation.[2–4] Over the years, the suitability of several PET radioisotopes for use as tracers has been advanced, along with their unique methods of production.[2,5] There are three major methods that can be used to produce radiometals – parent/progeny generators, nuclear reactors and cyclotrons.[2] For radioisotope production utilizing cyclotrons, radioisotopes can be produced using gas, liquid, or solid phase targets.[2,6] This review will focus on recent advancements in the use of solid targets.

The design of a solid target requires several considerations, and these factors influence its configuration and performance. Targets may be composed entirely of enriched and natural elements and alloys, and may be prepared as foils, disks or composites (through the electroplating, sputtering, sedimenting, or pressing of alloys and elements onto supporting metal substrates (target backing) such as gold, silver, tantalum, titanium, rhodium or niobium).[7–10] The specific design selected depends on factors such as substrate bond, heat transfer efficiency, ease of product isolation from the target material after irradiation, ease of target material recovery for enriched-material targets, product sensitivity to impurities and nuclear cross-section data.[8] An ideal target should be stable, allow a high rate of heat transfer, and possess favorable melting properties[6] since proton-induced irradiation generates significant amounts of heat in a small target area. When heat transfer and melting point are not suitable, innovations such as an oblique target arrangement as well as target alloying practices have been implemented to pacify these limitations.[6] The separation chemistry employed should be fast (*i.e.* less than one half-life of the product radionuclide) and efficient at separating the product from both the target material and co-produced impurities.[11] Commonly used separation techniques include are ion exchange chromatography, solid phase extraction (SPE) and thermochromatographic dry distillation, the schematics for which can be seen in Fig. 2, Fig. 3 and Fig. 4 respectively.

The radioisotopes covered in this review (see Table 1) can be produced on solid targets using small-to-medium sized, proton-accelerating cyclotrons with a maximum particle acceleration energy of 24 MeV. Production using this class of cyclotron was selected since these machines are the most prevalent in medical and research institutions. While the list of radioisotopes reviewed is a comprehensive one, the authors would like to highlight other PET radioisotopes such as ^{110m}In[12,13], ^{152}Tb,[13,14] ^{51}Mn,[15,16] ^{62}Cu[16–18] and ^{132}La[19,20] which are also available for production on the aforementioned cyclotrons, but were excluded from this review due to limitations. This review briefly discusses the biomedical application of each radionuclide while focusing mainly on the specifics of its production and purification procedures. Several recent reviews can provide more

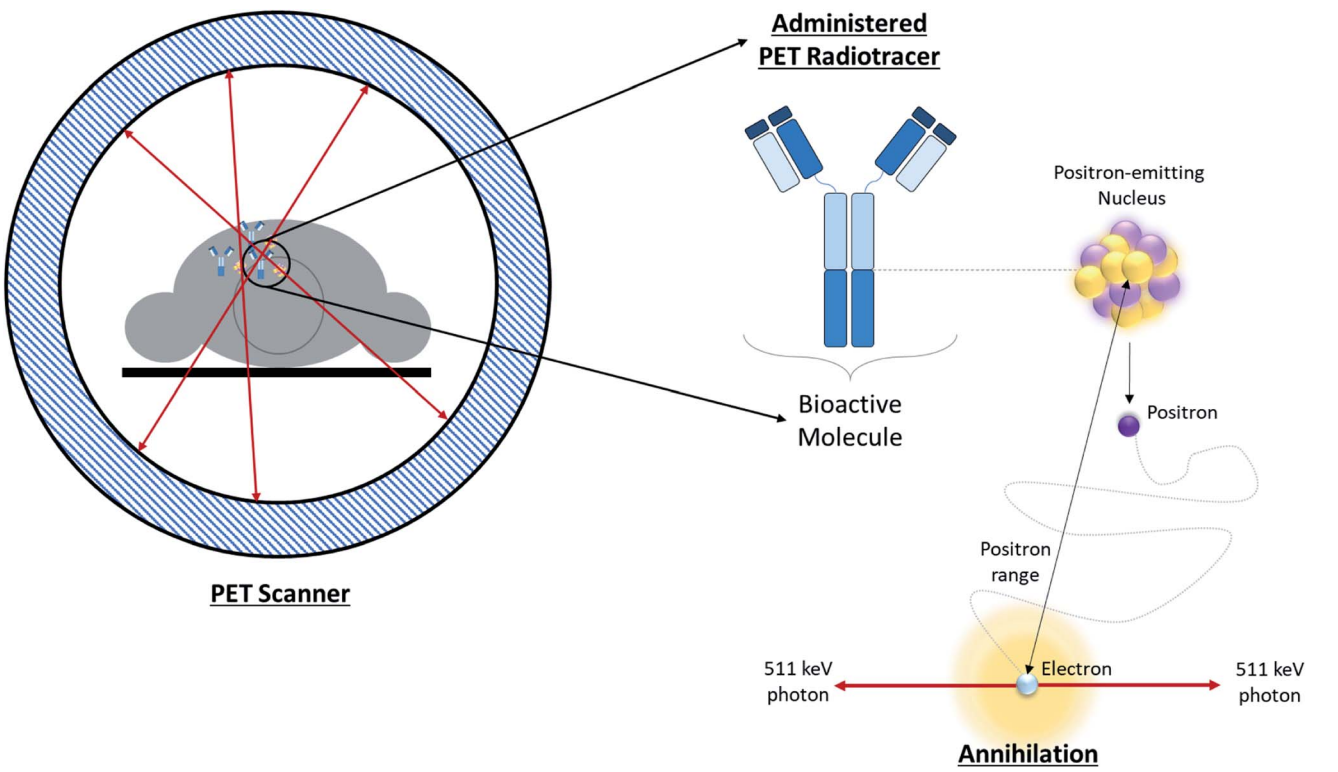

Fig. 1 Overview of PET. Schematic depicting positron annihilation in a patient undergoing a PET scan.

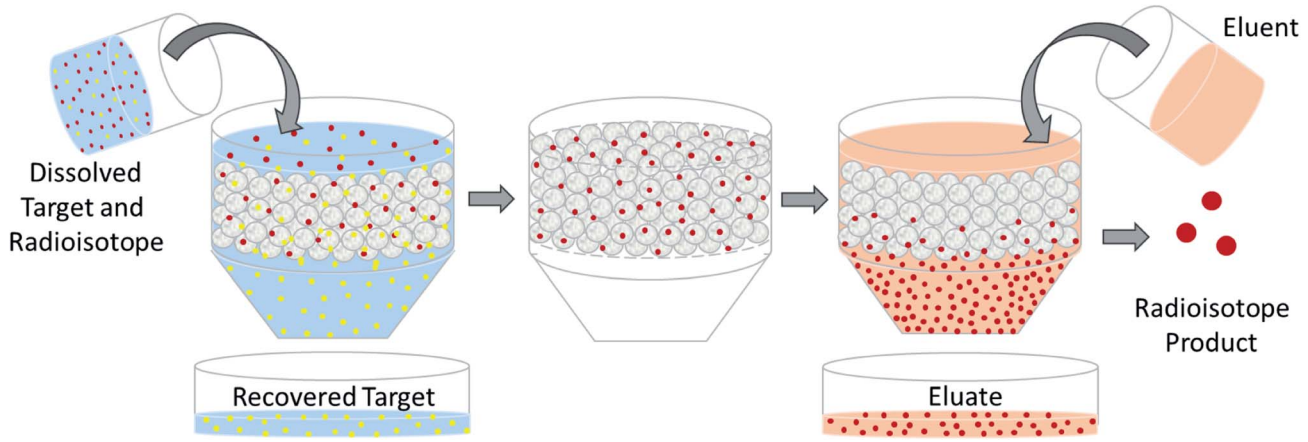

Fig. 2 Ion exchange chromatography. Schematic depicting the separation of dissolved PET radioisotopes from dissolved, unreacted target material after passage through an ion exchange column. The resin retains the PET radioisotope, and an eluent is used for its elution.

details on the applications of established and emerging PET radionuclides discussed herein ref. 21–23. A summary of the major nuclear and production properties of each radioisotope is provided in Table 1 for convenience. The nuclear information presented in this review was retrieved from the National Nuclear Data Center website by Brookhaven National Laboratory (https://www.bnl.gov).

List of PET radioisotopes

Halogens

Bromine: ^{75}Br, ^{76}Br

Applications. Since the early days of nuclear medicine, several bromine isotopes have been considered for therapy (auger emitting ^{77}Br), SPECT (^{80m}Br), and for PET imaging (^{75}Br and

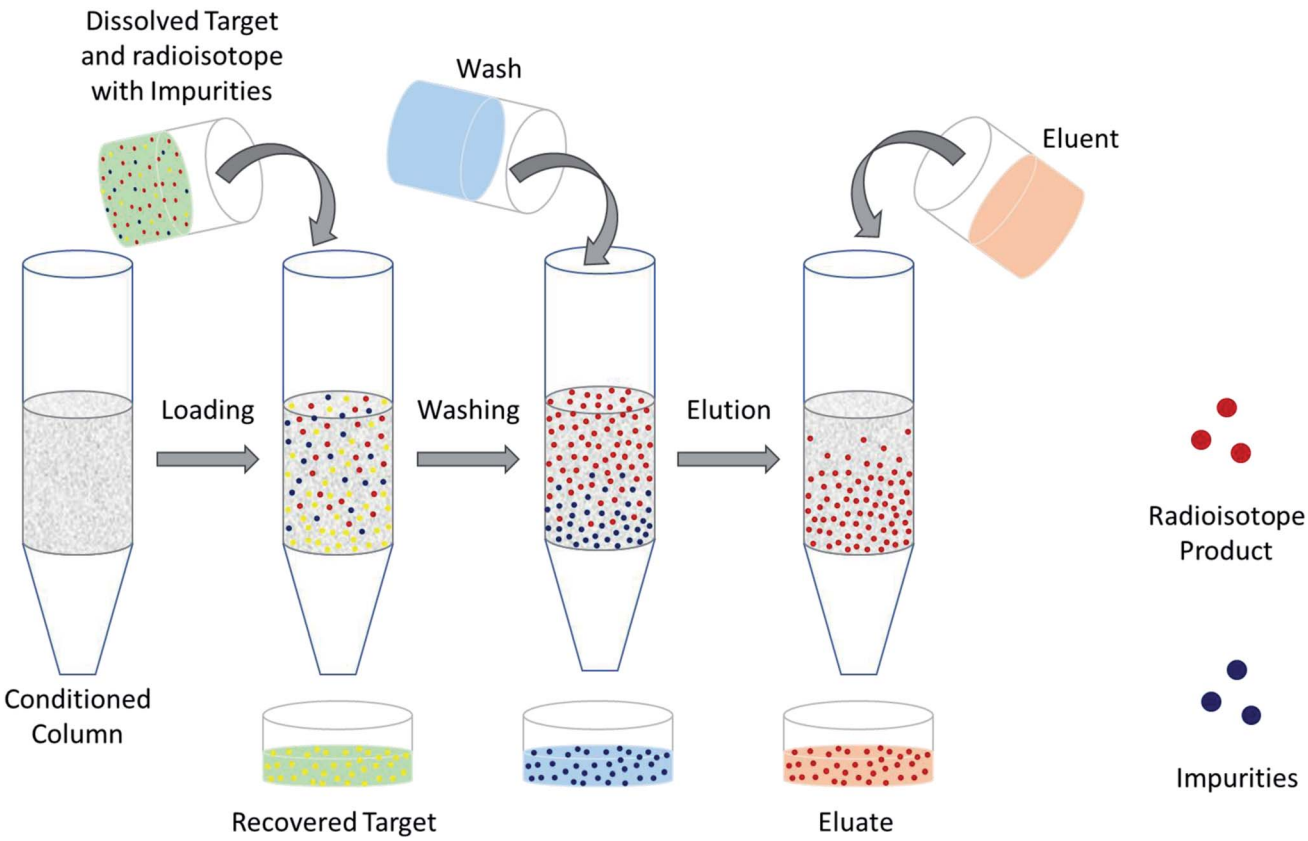

Fig. 3 Solid phase extraction. Schematic depicting the separation of dissolved PET radioisotopes from dissolved, unreacted target material after passage through a solid phase extraction column. The column retains the PET radioisotope and any impurities. Impurities are washed-off before elution is performed to obtain the PET radioisotope.

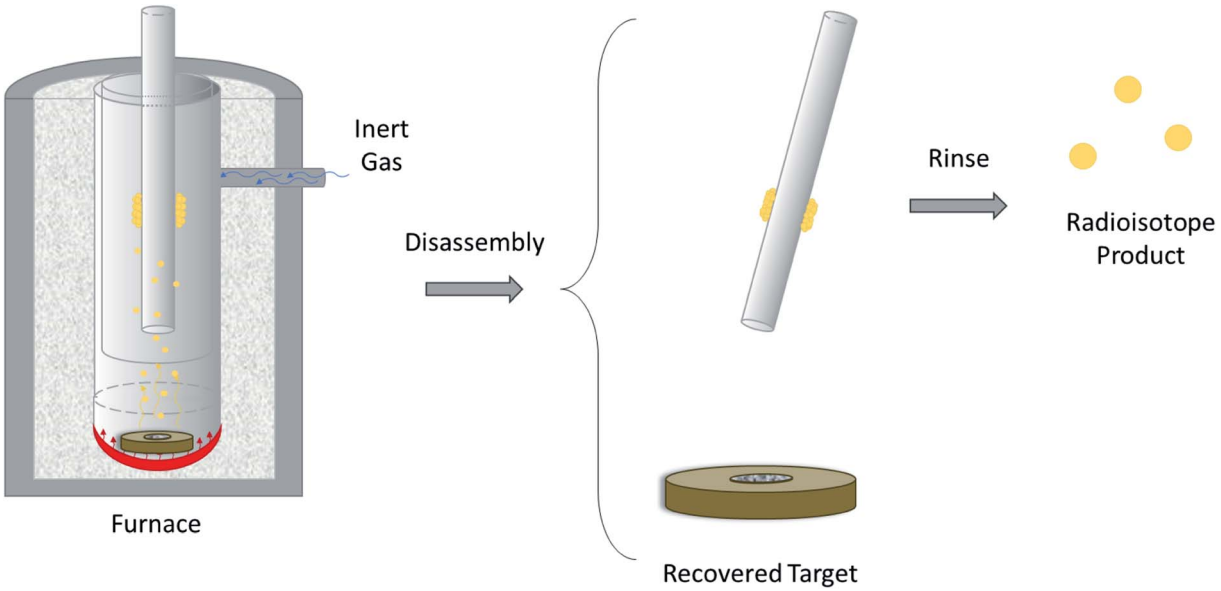

Fig. 4 Thermochromatographic dry distillation. Schematic depicting the separation of volatile PET radioisotopes from non-volatile target material after heating is performed in a furnace. The PET radioisotope condenses on a removable, cooler surface within the furnace. The radioisotope is removed from the surface using a rinse.

^{76}Br). With intermediary physicochemical properties between fluorine and iodine, radiobromines allow for fine-tuning molecular mass, volume, polarizability, and lipophilicity as alternatives to fluorine-18 (^{18}F; $t_{1/2}$: 109.8 min, 100% β^+) or radioiodines (see next section). Of the two positron emitting bromine isotopes, ^{75}Br ($t_{1/2}$: 96.7 min, 75% β^+, 25% EC), has the more favorable characteristics for PET applications with a larger yield of lower energy positrons and a lower number of other gamma-generating decay modes. While the long half-life daughter ^{75}Se ($t_{1/2}$: 119.8 d, 100.0% EC) warrants careful dose estimation, several ^{75}Br-labeled agents have undergone preclinical and clinical studies including cardiac fatty acid metabolism,[24] neuroreceptor mapping,[25–28] and glucose analogues.[29]

The other positron-emitting isotope is ^{76}Br ($t_{1/2}$: 16.2 h, 55% β^+, 45% EC). It has seen wider adoption primarily because it decays to stable ^{76}Se[1,30,31] and possesses a half-life well matched to protein pharmacokinetics as illustrated through ^{76}Br-labeled antibodies and their fragments for preclinical tumor imaging.[1] Beyond antibody radiolabeling, there are examples of ^{76}Br-labeled neuroimaging tracers,[32–34] peptides,[35] reporter gene studies,[36] and agents for studying sympathetic innervation.[37] Despite this there are limitations to using ^{76}Br-labelled tracers for PET imaging applications. Similar to radioiodine, it is prone to dehalogenation *in vivo* where it generally remains in blood circulation and slowly accumulates in the gastric mucosa.[38] The high levels of blood retention negatively affects image quality, particularly in blood rich organs (*i.e.* the heart and lungs) hours after the tracer has been administered.[1,38] Furthermore, bromide has a long biological half-life in human plasma (about 10 days) which makes elimination of labile [^{76}Br]Br$^-$ post-imaging problematic.[39] These concerns will surely be addressed as new ^{76}Br-labelled tracers are developed, given an expanded role of this isotope with new β^+ γ coincidence PET methodologies.[40,41] A recent review of the chemistry and applications of radiobromines[42] provides more insight into their applications.

Production. The primary nuclear reaction used to produce ^{75}Br on solid-target medical cyclotrons is the ^{76}Se(p,2n)^{75}Br nuclear reaction.[30,43–46] Although enriched elemental selenium has been used to produce solid targets for proton bombardment,[30,44–46] its low melting point and low thermal conductivity necessitates current restrictions to maintain target integrity during bombardment. Alloyed selenides such as NiSe, Ag_2Se, CuAgSe, Cu_2Se and PbSe[30,44,47] have been developed as suitable alternatives which permit irradiation at higher currents, significantly increasing yields. One drawback of selenium alloy targets is poor adherence to heat-conducting target backings.[44] The beam energy used for the production of ^{75}Br ranges from 24 to 21.5 MeV.[43,44] For this energy range, the theoretical ^{75}Br yields (assuming ^{76}Se-enriched targets), ranged from 1184 to 1480 MBq (μA h)$^{-1}$ (*i.e.* 32–40 mCi (μA h)$^{-1}$),[44] although production at higher energies (*i.e.* 28 to 22 MeV) provided yields up to three times greater.[30] The major impurity produced was ^{76}Br[43–45] although trace amounts of ^{72}As ($t_{1/2}$: 26.0 h, 87.8% β^+, 12.2% EC), ^{73}As ($t_{1/2}$: 80.3 d, 100.0% EC), ^{75}Se ($t_{1/2}$: 119.8 d, 100.0% EC) and ^{77}Br ($t_{1/2}$: 57.0 h, 0.7% β^+, 99.3% EC) have been reported.[44]

There are several reactions that can be used to produce ^{76}Br, however few can be carried out using lower-energy medical cyclotrons.[46] Nevertheless, a feasible production route is the ^{76}Se(p,n)^{76}Br nuclear reaction, which occurs in the 16 to 8 MeV beam energy range.[48] Like ^{75}Br, the target was composed of an enriched selenium alloy, specifically Cu_2Se[48,49] or NiSe.[47] Bombarding a Cu_2Se target with beam energies ranging from 16 to 8 MeV, the yield of ^{76}Br ranged from 65 to 70 MBq (μA h)$^{-1}$ (*i.e.* 1.8 to 2.1 mCi (μA h)$^{-1}$) at end of bombardment (EOB).[48] The

Table 1 Properties of emerging and commonly used PET radionuclides

		Nuclear properties					Production conditions			
Element	Isotope	Half-life	Mode of decay (%)	Avg. β^+ energy, keV	β^+ endpoint energy, keV (%)	Principal γ energies, keV (Abs. %)	Major nuclear reactions	Beam energy, MeV	Target	Max. reported yield, MBq $(\mu A\ h)^{-1}$
Arsenic (As)	72	26.0 h	β^+ (87.8) EC (12.2)	1117 1528	2500 (64.2) 3334 (16.3)	511 (176.4), 630 (8.1), 834 (81.0), 1464 (1.13)	^{72}Ge(p,n)^{72}As	18–8	Natural or enriched GeO_2 on Cu or Nb, Ge foil	90
Bromine (Br)	75	96.7 min	β^+ (75.0) EC (25.0)	773, 708, 904	1753 (53.0), 1612 (4.9), 2040 (4.0)	511 (149.1),141 (6.6), 287 (88.0), 428 (4.4)	^{76}Se(p,2n)^{75}Br	24–21.5	Enriched Se, enriched selenides (*i.e.* Ag_2Se, CuAgSe, Cu2Se, PbSe)	1480
	76	16.2 h	β^+ (55.0) EC (45.0)	1532, 375, 1800	3382 (25.8), 871 (6.3), 3941 (6.0)	511 (109), 559 (74.0), 657 (15.9), 1854 (147)	^{76}Se(p,n)^{76}Br	16–8	Enriched Se, enriched selenides (*i.e.* Cu_2Se)	70
Copper (Cu)	60	23.7 min	β^+ (93.0) EC (7.0)	872, 1325, 840	1982 (49.0), 2947 (15.0), 1912 (11.6)	511 (185.0), 826 (21.7), 1333 (88.0), 1792 (45.4)	^{60}Ni(p,n)^{60}Cu	14.7	Natural or enriched Ni on Au	2146
	61	3.3 h	β^+ (61.0)	524, 399	1216 (51.0), 933 (5.8)	511 (123.0), 67 (4.2), 282 (12.2),	^{61}Ni(p,n)^{61}Cu	14.7–9	Enriched Ni on Au	281
			EC (39.0)			656 (10.8)	^{64}Zn(p,α)^{61}Cu	17.6–11.7	Natural or enriched Zn	13
	64	12.7 h	β^+ (17.6) β^- (38.5) EC (43.9)	278	653 (17.6)	511 (35.2), 1346 (0.5)	^{64}Ni(p,n)^{64}Cu	15–10	Enriched Ni on Au or Rh	5883
Cobalt (Co)	55	17.5 h	β^+ (76.0) EC (24.0)	649, 436	1499 (46.0), 1021 (25.6)	511 (152.0), 477 (20.2), 931 (75.0), 1409 (16.9)	^{56}Fe(p,2n)^{55}Co ^{58}Ni(p,α)^{55}Co	23.5–16 16–15	Enriched Fe Enriched Ni, enriched Ni on Ag or Au	236
Gallium (Ga)	66	9.5 h	β^+ (57.0) EC (43.0)	1904, 397	4153 (51.0), 924 (3.7)	511 (114.0), 834 (5.9), 1039 (37.0), 2752 (22.7)	^{66}Zn(p,n)^{66}Ga	15–6	Natural or enriched Zn on Au or Ag	700
	68	67.7 min	β^+ (88.9) EC (11.1)	836, 353	1899 (87.7), 822 (1.2)	511 (177.8), 1077 (3.2), 1261 (0.1), 1883 (0.1)	^{68}Zn(p,n)^{68}Ga	14–11	Enriched Zn, enriched Zn on Al, Au or Ag	1380
Iodine(I)	124	4.2 d	β^+ (22.7) EC (77.3)	687, 975	1535 (11.7), 2138 (10.7)	511 (45.0), 603 (62.9), 723 (10.4), 1691 (11.2)	^{124,125}Te(p,*x*n)^{124}I	22–5	Natural or enriched Te, natural or enriched TeO_2	111
Manganese (Mn)	52g	5.6 d	β^+ (29.4) EC (70.6)	242	575 (29.4)	511 (58.8), 744 (90.0), 936 (94.5), 1434 (100.0)	^{52}Cr(p,n)^{52g}Mn	20–10	Natural Cr, natural Cr on Cu or Ag	9.6
Niobium (Nb)	90	14.6 h	β^+ (53.0) EC (47.0)	662, 726	1500 (51.0), 1641 (2.0)	511 (102.0), 142 (66.8), 1129 (92.7), 2319 (82.0)	^{90,91}Zr(p,*x*n)^{90}Nb	19–7	Natural Zr, enriched ZrO_2 on Cu	596
Scandium (Sc)	44g	4.0 h	β^+ (94.3) EC (5.7)	632	1474 (94.3)	511 (188.5), 1157 (99.9), 1499 (0.9)	^{44}Ca(p,n)^{44g,m}Sc	18–6	Natural or enriched Ca, enriched CaO_3	50
Technetium (Tc)	94m	52 min	β^+ (70.2) EC (29.8)	1094, 639, 405	2439 (67.6), 1446 (0.9), 917 (0.9)	511 (140.3), 871 (94.2)	^{94}Mo(p,n)^{94m}Tc	13–6	Natural Mo, enriched MoO_3	111
Titanium (Ti)	45	184.8 min	β^+ (84.8) EC (15.2)	439	1040 (84.8)	511 (169.6), 720 (0.2), 1408 (0.1)	^{45}Sc(p,n)^{45}Ti	16–8	Natural Sc	422
Yttrium (Y)	86g	14.7 h	β^+ (31.9) EC (68.2)	535, 681, 883	1221 (11.9), 1545 (5.6), 1988 (3.6)	511 (64.0), 628 (32.6), 1077 (82.5), 1153 (30.5)	^{86}Sr(p,n)^{86g}Y	15.1–11	Enriched $SrCO_3$ or SrO	166
Zinc (Zn)	63	38.5 min	β^+ (92.7) EC (7.3)	1042, 733, 600	2345 (80.3), 1675 (7.0), 1382 (4.9)	511 (185.5), 670 (8.2), 962 (6.5), 1412 (0.8)	^{63}Cu(p,n)^{63}Zn	16–6	Natural or enriched Cu	2470
Zirconium (Zr)	89	78.4 h	β^+ (22.7) EC (77.3)	396	902 (22.7)	511 (45.5), 909 (99.0), 1713 (0.7), 1745 (0.1)	^{89}Y(p,n)^{89}Zr	14–9	Natural Y, natural Y_2O_3 on Cu	58

Table 2 Production and purification parameters for ^{75}Br and ^{76}Br

Radioisotope	^{75}Br, ^{76}Br
Target material	Elemental selenium, selenides (NiSe, Ag_2Se, CuAgSe, Cu_2Se, PbSe)
Product purity	—
Major impurities	^{76}Br, ^{72}As, ^{73}As, ^{75}Se, ^{77}Br
Separation method	Thermochromatographic dry distillation (300–1100 °C in Ar; water or ethanol for precipitate dissolution; NaOH trap)
Product separation yield	65–75%
Target recovery yield	(100 − x)%, where 'x' is no. of times reused

primary impurity produced for this production route was ^{77}Br (2%).[30,46]

Product purification and target recovery. The primary method used to isolate bromine from irradiated selenium was thermochromatographic dry distillation.[30,43,44,46,48] This procedure required heating the selenide targets in an enclosed, oxygen-free apparatus such as a furnace or dedicated distillation vessel. The distillation temperature depended on the type of target being processed, with 300 °C being ideal for distillation of bromine from elemental selenium targets[43,44] and temperatures ranging from 1090 to 1100 °C being ideal for the selenide targets.[30,48] To ensure an oxygen-free environment, an inert gas such as argon was continuously passed through the system. In addition to reducing oxygen exposure, the argon gas mobilizes vaporized bromine and selenium gases generated from the distillation out of the furnace and into a cold trap for collection. The vaporized selenium was the first to condense along the walls of the tubing at temperatures between 120 and 215 °C,[44] while the bromine began to condense closer to room temperature. Any uncondensed bromine can be collected by bubbling the gas stream through water[44] or a dilute NaOH solution.[48] The condensed bromine can be removed by washing with pure water or absolute ethanol.[30,44] Once cooled, the heated targets can be recycled and repeatedly irradiated, typically up to 20 times with <1% target material loss per run.[30,48] The product separation yield for the process ranged from 65–75%.[48]

Summary. Table 2 below summarizes key production and purification parameters for ^{75}Br and ^{76}Br not hitherto mentioned in Table 1.

Iodine: ^{124}I

Applications. Apart from ^{99m}Tc, radioiodines are the most commonly used radionuclides in nuclear medicine. Complementary to the near ideal SPECT isotope ^{123}I ($t_{1/2}$: 13.2 h, 100.0% EC), the positron emitting ^{124}I ($t_{1/2}$: 4.2 d, 22.7% β^+, 77.3% EC) has been used extensively in immunoPET imaging and other protein-based PET applications due to its well-understood radiochemistry and long half-life.[1,50] Thus far, ^{124}I has been used for cancer diagnosis, monitoring and treatment planning, as well as mechanistic, and pharmacokinetic studies.[51–54] Beyond antibodies, ^{124}I labelled peptides and small molecules targeting neurotransmitters systems, tumor hypoxia, prostate specific membrane antigen (PSMA), and neuroinflammation have also been investigated in humans.[55–57] However, the use of ^{124}I is not without its limitations, not the least of which is its comparatively low positron yield at a high end-point energy. This results in low spatial resolution[58] which may be addressed through hybrid imaging with PET/MR instruments possessing strong magnetic fields.[59] Another drawback is the large number of gammas released from electron capture, increasing patient radiation dose, and further limiting image resolution. These can be corrected for with special software[1,3] and may be turned into an advantage using the aforementioned β^+/γ coincidence tomography.[41] To avoid high doses to the thyroid gland from the high energy positron and gammas, ideally the attachment of ^{124}I to biomolecules is kinetically inert.[60] Readers are referred to recent reviews on the radiochemistry and application of radioiodines for more information.[23,42] Taking advantage of increased interest in theranostic radiopharmaceuticals, ^{124}I may see a surge in upcoming years as a companion to ^{131}I ($t_{1/2}$: 8.02 d, β^-: 971 keV) or used for therapy itself (70% absorbed dose of ^{131}I.[61]

Production. While ^{124}I can be produced through a number of different nuclear reaction pathways, however the most feasible production *via* low-energy proton cyclotron is through the ^{124,125}Te(p,xn)^{124}I nuclear reactions. The radioisotope can be produced through the irradiation of natural tellurium (isotopic composition: 0.09% ^{120}Te, 2.55% ^{122}Te, 0.89% ^{123}Te, 4.74% ^{124}Te, 7.07% ^{125}Te, 18.84% ^{126}Te, 31.74% ^{128}Te, 34.08% ^{130}Te) metalloid targets, >98% enriched ^{124,125}Te metalloid targets, and enriched tellurium oxides electro-deposited or melted onto platinum or tantalum substrates. The optimum beam energy range used for irradiation can range from 14 to 5 MeV for ^{124}Te-based targets, and 22 to 4 MeV for ^{125}Te-based targets. The primary impurities produced during bombardment using ^{124}Te-based targets were ^{123}I ($t_{1/2}$: 13.2 h, 100.0% EC), ^{125}I ($t_{1/2}$: 59.4 d, 100.0% EC), ^{126}I ($t_{1/2}$: 12.9 d, 1.0% β^+, 47.3% β^-, 51.7% EC) and ^{130}I ($t_{1/2}$: 12.4 h, 100.0% β^-), while the primary impurities for ^{125}Te-based targets are ^{123}I and ^{125}I.[9,46,54,62,63] For the ^{124}Te(p,n)^{124}I nuclear reaction within the 14 to 7 MeV energy range, reported yields ranged from 5 to 21 MBq (μA h)$^{-1}$ (*i.e.* 0.1 to 0.6 mCi (μA h)$^{-1}$) with major impurities equaling less than 1%. For the ^{125}Te(p,2n)^{124}I nuclear reaction within the 22 to 4 MeV energy range, reported yields ranged from 43 to 111 MBq (μA h)$^{-1}$ (*i.e.* 1.2 to 3.0 mCi (μA h)$^{-1}$) with impurities comprising as much as 13% of the final product.[54,62–64]

Product purification and target recovery. The preferred method for separating the radioiodine from the post-bombarded tellurium target material is *via* dry (thermochromatographic) distillation,[46,54,63] which is facilitated by the favorable melting and solidification properties of TeO_2. Conventional dry distillation was carried out using a ventilated quartz tube where the irradiated TeO_2 was heated to temperatures between 670 to 820 °C for periods ranging from 5 to 20 min in carrier gases of either air, argon, helium, or oxygen. This approach aimed to extract as much of the iodine product using a NaOH trap, however, any prematurely condensed iodine can be removed *via* dissolution using a weak buffer solution. To minimize tellurium evaporation, Al_2O_3/quartz wool was integrated into the distillation setup.[63] The separation efficiency for the dry distillation stage ranged from 80% to 95%.[54] Wet chemistry methods were

also used to chemically isolate iodine from the tellurium targets, but these methods were less preferred due to product dilution in the final solution. The process was carried out in two stages, with the first being a target dissolution stage using an oxidizing alkali, and the second a reduction stage facilitated by the addition of aluminum powder.[9]

After the iodine has been extracted, the spent tellurium targets can be recycled. Metallic tellurium targets can be dissolved in a mixture of hydrogen peroxide and hydrochloric acid, and the resulting solution can subsequently be reduced using either hydrogen bromide or a mixture of hydrazine and sodium sulfite. Reduction *via* the former recovered tellurium in the form of tellurite, while the latter facilitated the recovery of metallic tellurium.[9] For tellurium oxide targets, a multistage process involving vacuum distillation, acid dissolution and chemical precipitation was used to recover metallic tellurium.[9] In general, the recovery yields for tellurium-based targets range from 60 to 90%.[54] However, despite the innovations in tellurium recovery, ^{124}I production is still negatively affected by high target material costs.[62]

Summary. Table 3 summarizes key production and purification parameters for ^{124}I not previously mentioned in Table 1.

Transition metals

Copper: ^{60}Cu, ^{61}Cu and ^{64}Cu

Applications. Copper has many positron-producing radionuclides (*i.e.* ^{60}Cu ($t_{1/2}$: 23.7 min, 93.0% β^+, 7.0% EC), ^{61}Cu ($t_{1/2}$: 3.3 h, 61.0% β^+, 39.0% EC) and ^{64}Cu ($t_{1/2}$: 12.7 h, 17.6% β^+, 38.5% β-, 43.9% EC)) that are finding use in PET applications primarily due to their well-established coordination chemistry.[10] Although less frequently utilized, ^{60}Cu and ^{61}Cu have been used to label various bioactive molecules for hypoxia and blood flow studies.[17,21,65]

The most commonly used copper radioisotope is ^{64}Cu, with the first-in-human use as [^{64}Cu]ASTM for tumor hypoxia.[66] There are several characteristics that make ^{64}Cu well suited for PET imaging. Besides its well elucidated chemistry, its favorable half-life allows it to be used for radiolabeling various targeting vectors like peptides, antibodies, and nanoparticles.[1,10] Additionally, the positron energy for ^{64}Cu (mean: 278 keV, max: 653 keV) is comparable to ^{18}F (mean: 250 keV, max: 634 keV), leading to similar positron range and excellent spatial resolution.[67] With respect to use in immunoPET, there exists some dissonance between radiolabeling conditions and antibody stability. Moreover, some ^{64}Cu radiotracers were found to be susceptible to metabolism in the liver, which permits transchelation of the radioisotope with other copper-binding proteins such as Cu/Zn superoxide dismutase (Cu/Zn SOD) in the liver and metallothionein in the blood.[1,3,68] These limitations may be overcome with improved chelator technology.[69,70] Lastly, it warrants mentioning the potential theranostic pairing with ^{67}Cu ($t_{1/2}$: 2.58 d, β^-: 100%, avg. E_{β^-}: 141 keV) which makes it ideal for radioimmunotherapy monitoring.[71]

Production. As ^{60}Cu is typically produced *via* the ^{60}Ni(p,n)^{60}Cu nuclear reaction, occurring with natural nickel (isotopic composition: 68.08% ^{58}Ni, 26.22% ^{60}Ni, 1.14% ^{61}Ni, 3.63% ^{62}Ni, 0.93% ^{64}Ni) and enriched ^{60}Ni targets when bombarded with a beam energy of 14.7 MeV.[65] For the 14.7 MeV bombardment of >99% enriched ^{60}Ni electroplated on a gold target backing, the yield at EOB was 2146 MBq (μA h)$^{-1}$ (*i.e.* 58 mCi (μA h)$^{-1}$) with the primary impurities produced to include ^{61}Cu ($t_{1/2}$: 3.3 h, 61.0% β^+, 39.0% EC) (0.05%) and ^{57}Co ($t_{1/2}$: 271.7 d, 100.0% EC) (0.025%).[65] When bombardment was carried out using natural nickel targets for similar conditions in the same study, EOB yields of 291 MBq (μA h)$^{-1}$ (*i.e.* 7.9 mCi (μA h)$^{-1}$) and 385 MBq (μA h)$^{-1}$ (*i.e.* 10.4 mCi (μA h)$^{-1}$) were reported along with the presence of ^{55}Co ($t_{1/2}$: 17.5 h, 76.0% β^+, 24.0% EC) (0.65%) and ^{61}Cu (0.60%) as the major impurities.[65]

Both the ^{61}Ni(p,n)^{61}Cu[65,72] and ^{64}Zn(p,α)^{61}Cu[17,72] nuclear reactions have been reported for the production of ^{61}Cu. Production *via* ^{61}Ni(p,n)^{61}Cu required proton optimum beam energies ranging from 14.7 to 9 MeV and enriched ^{61}Ni targets. For the 14.7 MeV bombardment of >99% enriched ^{61}Ni electroplated onto a gold target substrate with a thickness of 118 μm and diameter of 5 mm, the ^{61}Cu yield at EOB was 281 MBq (μA h)$^{-1}$ (*i.e.* 7.6 mCi (μA h)$^{-1}$) while the primary impurity produced was ^{58}Co ($t_{1/2}$: 70.9 d, 14.9% β^+, 85.1% EC) (0.04%).[65] In the same study, ^{60}Ni(d,n)^{61}Cu reactions were investigated but produced lower yields at higher per bombardment costs. Alternatively, ^{61}Cu can be produced using the ^{64}Zn(p,α)^{61}Cu nuclear reaction. The reaction has been investigated with natural zinc (isotopic composition: 49.17% ^{64}Zn, 27.73% ^{66}Zn, 4.04% ^{67}Zn, 18.45% ^{68}Zn, 0.61% ^{70}Zn) foils and enriched ^{64}Zn electroplated on to gold, silver or aluminum substrates with beam energies ranging from 17.6 to 11.7 MeV (maximum production occurs circa 14.5 MeV).[17] When >99% enriched ^{64}Zn was bombarded with 14.5 MeV protons, the yield of ^{61}Cu was 13 MBq (μA h)$^{-1}$ (*i.e.* 0.4 mCi (μA h)$^{-1}$) with a purity exceeding 95%.[17] Despite having completed similar experiments using natural zinc foil targets in the same study, the results were too

Table 3 Production and purification parameters for ^{124}I

Radioisotope	^{124}I
Target material	Natural and enriched tellurium, enriched tellurium oxide
Product purity	87–>99%
Major impurities	^{123}I, ^{125}I, ^{126}I, ^{130}I
Primary separation method	Thermochromatographic dry distillation (670–820 °C in air, Ar, He or O_2; weak buffer for precipitated dissolution; NaOH trap)
Product separation yield	80–95%
Target recovery yield	60–90%

variable to draw valid conclusions. The primary impurities produced during the bombardment of zinc targets were ^{66}Ga ($t_{1/2}$: 9.5 h, 57.0% β^+, 43.0% EC), ^{67}Ga ($t_{1/2}$: 3.3 d, 100.0% EC) and ^{68}Ga ($t_{1/2}$: 67.7 min, 88.9% β^+, 11.1% EC).[17] Based on the data generated, ^{61}Cu production from the bombardment of nickel was found to be more efficient than production using zinc. However, the former production route can be expensive due to the high cost associated with enriched ^{61}Ni. Since enriched ^{64}Zn is significantly cheaper than enriched ^{61}Ni, the production of ^{61}Cu from zinc targets has found some consideration as an alternative route.[17]

^{64}Cu is primarily produced *via* the ^{64}Ni(p,n)^{64}Cu nuclear reaction.[9,62] The solid target used for the production is typically enriched ^{64}Ni that has been electroplated onto a gold[62,73–77] or rhodium[10] target backing substrate. Although the threshold for the reaction is 2.5 MeV, production of ^{64}Cu has been reported for beam energies ranging from 15 to 10 MeV since this range offers the highest yields.[62] Numerous yields for the production of ^{64}Cu have been reported in the literature. McCarthy *et al.*[76] reported yields ranging from 85 to 185 MBq (μA h)$^{-1}$ (*i.e.* 2.3 to 5 mCi (μA h)$^{-1}$) when gold substrates electroplated with >95% ^{64}Ni (thicknesses ranging from 132 to 311 μm) were bombarded with a 15.5 MeV proton beam, while McCarthy *et al.*[65] reported yields of 296 MBq (μA h)$^{-1}$ (*i.e.* 8 mCi (μA h)$^{-1}$) for greater purity targets of similar design (*i.e.* >99% ^{64}Ni electroplated onto a gold substrate with a thickness of 215 μm and diameter of 5–6 mm) irradiated at 14.7 MeV. Obata *et al.*[77] reported yields ranging from 22 to >111 MBq (μA h)$^{-1}$ (*i.e.* 0.6 to >3 mCi (μA h)$^{-1}$) when they bombarded gold substrates that were electroplated with 94.8% ^{64}Ni with a 12 MeV proton beam. More recently, a saturation yield of 5883 MBq (μA h)$^{-1}$ (*i.e.* 159 mCi (μA h)$^{-1}$) has been reported by Avila-Rodriguez *et al.* (2007) when they bombarded gold substrates electroplated with >95% enriched ^{64}Ni with an 11.4 MeV proton beam. The primary impurity produced for this reaction is ^{55}Co ($t_{1/2}$: 17.5 h, 76.0% β^+, 24.0% EC) (0.012%).[65] However, other relevant impurities include ^{57}Ni ($t_{1/2}$: 35.6 h, 43.6% β^+, 56.4% EC), ^{56}Co ($t_{1/2}$: 77.2 d, 19.7% β^+, 80.3% EC), ^{57}Co ($t_{1/2}$: 271.7 d, 100.0% EC) and ^{58}Co ($t_{1/2}$: 70.9 d, 14.9% β^+, 85.1% EC).[73]

Product purification and target recovery. Isolation of the copper product from the target material begins with target dissolution in strong acid (*i.e.* 6 M HNO_3 or 6 N HCl at temperatures ranging from 90 to 100 °C (Jeffery *et al.* 2012). The acidic solution is passed through an anion exchange column filled with AG1-X8 resin which retains the copper product along with the nickel target material and any cobalt impurities present. The nickel target material is eluted first using 6 N HCl[75,76] for HCl-dissolved targets, or 0.2 M HCl in 96% methanol[74] for HNO_3-dissolved targets. The cobalt impurity fraction retained by the column can be eluted with 4 M HCl[75] for HCl-dissolved targets, or 0.3 M HCl in 72% ethanol[74] for HNO_3-dissolved targets. Finally, the copper product can be eluted using dilute acid (*i.e.* 0.1–0.5 M) or distilled water[75,76] for HCl-dissolved targets, or 0.3 M HCl in 40% ethanol[74] for HNO_3-dissolved targets. Separation yields exceeding 95% have been reported for the process.[75]

Implementation of a dedicated recycling scheme for ^{60}Ni recovery is not typical due to its low material cost,[65] which stems from the large natural abundance of the isotope. However, recycling of enriched ^{64}Ni is necessary to keep production costs down. Several methods have been developed for ^{64}Ni recovery. The method described by Obata *et al.*[77] made use of two heating stages conducted in series. In the first heating stage, the solution containing the eluted nickel was evaporated to dryness at 150 °C before it was rehydrated with distilled water. In the second heating stage, the rehydrated solution was heated at 900 °C for 24 h. This resulted in the formation of ^{64}NiO which was then used for the preparation of future targets. The minimum recycling efficiency for this process was 94%. A second method was discussed by McCarthy *et al.*,[76] and required several evaporation and acid dissolution steps be carried out in series. The first two acid dissolution steps were performed with HNO_3 and the final acid dissolution step was performed with H_2SO_4. After H_2SO_4 dissolution, the solution was diluted and the pH was adjusted to 9 with the addition of concentrated NH_4OH. The solution was available for electroplating after the addition of ammonium sulfate and a final dilution with deionized water. The overall efficiency of this recovery process exceeded 90%.

For the case of ^{61}Cu production from zinc targets, Rowshanfarzad *et al.*[72] and Asad *et al.*[17] outlined a method which made use of multiple column separation stages in series. The zinc portion of the targets were dissolved in 10 M HCl at room temperature before passing through a cation exchange column filled with AG 50W-X8 resin (200–400 mesh). The column retained the copper product, the gallium impurities, and the unreacted zinc target material. The copper product and zinc target materials were eluted with 10 M HCl and the eluant was passed through an AG 1-X8 anion exchange column (200–400 mesh). Both the copper product and zinc target material were retained, and the copper product was selectively eluted with 2 M HCl. In order to recycle the zinc target material (as in the case of enriched targets), the column can be eluted with 0.5 M HCl.[17] This solution was then evaporated to dryness before 6 M H_2SO_4 was added to digest any resin residues from the prior chromatography stages. The evaporation/digestion stage was repeated before the recovered zinc was finally reconstituted as an electroplating solution. The overall yield for the ^{64}Zn recovery process was about 90%.[17]

Summary. Table 4 summarizes key production and purification parameters for ^{60}Cu, ^{61}Cu and ^{64}Cu not mentioned in Table 1.

Cobalt: ^{55}Co

Applications. Cobalt is a human micronutrient and component of the essential vitamin B_{12} (cobalamin). As a potential competitor radionuclide to ^{64}Cu, ^{55}Co ($t_{1/2}$: 17.5 h, 76.0% β^+, 24.0% EC) has been shown to mimic calcium intake in infarcted brain tissue. This property makes it useful in the imaging of recent cerebral brain damage resulting from cerebral tumors, stroke and other brain injuries.[78–81] Recent reports have demonstrated high resolution PET images obtained with peptide and affibody chelates of ^{55}Co.[82,83] Ionic ^{55}Co species are residualizing radiotracers. Significant amounts of ^{55}Co can accumulate in organs such as the bladder, liver and kidney[84] with the majority eliminated or decayed three days post-injection. ^{55}Co has also shown great promise in the field of

immunoPET imaging and has been used to label an anti-EGFR affibody[82] as well as several peptides.[83,85] Unfortunately, widespread clinical use of this isotope may be hampered as ^{55}Co decays into ^{55}Fe ($t_{1/2}$: 2.73 years) while releasing large amounts of high energy gamma rays from electron capture in the process.[1] Nonetheless, it remains a valuable tool for preclinical PET investigations.

Production. There are two major nuclear reactions available to produce ^{55}Co on small medical cyclotrons by utilizing either the ^{56}Fe(p,2n)^{55}Co[81,86,87] or the ^{58}Ni(p,α)^{55}Co.[81,88,89] Production *via* ^{56}Fe(p,2n)^{55}Co involved irradiating ^{56}Fe-enriched iron foils[87] with a minimum proton beam energy of about 16 MeV,[86,87] although the reaction peaks at an energy near 23.5 MeV.[87] However, this production route was undesirable since significant amounts of the chemically-inseparable ^{56}Co ($t_{1/2}$: 77.2 d, 19.7% β^+, 80.3% EC) impurity was also co-produced.[81] The ^{58}Ni(p,α)^{55}Co production route can be carried out through the bombardment of natural nickel (isotopic composition: 68.08% ^{58}Ni, 26.22% ^{60}Ni, 1.14% ^{61}Ni, 3.63% ^{62}Ni, 0.93% ^{64}Ni) foils[89] or enriched ^{58}Ni-electroplated onto silver[88] or gold[81] disk substrates. Irradiations have been carried out using proton beams with energies of about 16 MeV (ref. 88 and 90) to 15 MeV.[81] The primary impurities produced during irradiation were ^{57}Co ($t_{1/2}$: 271.7 d, 100.0% EC), ^{58}Co ($t_{1/2}$: 70.9 d, 14.9% β^+, 85.1% EC) and ^{57}Ni ($t_{1/2}$: 35.6 h, 43.6% β^+, 56.4% EC), particularly when natural nickel targets were used for the production.[89] The saturation yield of ^{55}Co when natural nickel foils were bombarded with a beam energy of 16 MeV was 236 MBq (μA h)$^{-1}$ (*i.e.* 6.3 mCi (μA h)$^{-1}$) at EOB with purity exceeding 97%.[89] ^{55}Co yields from 16 MeV proton beam bombardments of >99% ^{58}Ni-electroplated gold disk substrates resulted in 9.3 MBq (μA h)$^{-1}$ (*i.e.* 0.3 mCi (μA h)$^{-1}$) with a purity exceeding 92%.[88]

Product purification and target recovery. Column-based separation techniques have been used to isolate cobalt from the nickel targets after heated dissolution with concentrated HCl.[81,88,89] The first example used an AG1-X8 anion exchange resin[81,89] which retained the cobalt product when the acidic target solution was passed through. Dilute HCl with concentrations ranging from 0.4–0.5 M (ref. 81 and 89) could be used to elute the cobalt product from the resin. Another stationary phase, DGA branched resin,[88] was demonstrated to selectively release ^{55}Co upon elution with 3 M HCl. The overall separation efficiency for the process generally exceeded 90%.[88,89] If the method used for target preparation was the electroplating of enriched ^{58}Ni on a metal disk substrate, ^{58}Ni was recovered with a 94% efficiency from the spent target solution using a series of drying and chemical cleaning stages before finally being reconstituted as an electroplating solution.[88]

Summary. Table 5 summarizes key production and purification parameters for ^{55}Co not mentioned in Table 1.

Manganese: ^{52g}Mn

Applications. A considerable amount of interest in the use of ^{52g}Mn ($t_{1/2}$: 5.6 d, 29.4% β^+, 70.6% EC) in PET applications has developed since its first use as a myocardial perfusion PET agent in 1985.[91] The radionuclide has been used in several preclinical imaging studies, including murine 4T1 xenografts, functional β-cells in type 1 and type 2 diabetes, and neural imaging in primates.[22,92] The interest in ^{52g}Mn stems from its decay characteristics, ease of production, and its potential to act as a surrogate to non-invasively quantify MR contrast agent.[93] The ^{52g}Mn radioisotope has a long half-life which facilitates late time-point studies up to 2 to 3 weeks following tracer administration, making it suitable for ImmunoPET applications.[1,94] Additionally, positron decay occurs at a low positron energy (β^+ E_{max}: 575 keV), promoting high resolution imaging that is comparable to ^{18}F.[93] Despite its numerous advantages, caution is exercised when using ^{52g}Mn for PET applications since it has several high energy gamma emissions (*i.e.* 744, 935, and 1434

Table 4 Production and purification parameters for ^{60}Cu, ^{61}Cu and ^{64}Cu

Radioisotope		^{60}Cu, ^{61}Cu, ^{64}Cu
Target material		Natural and enriched nickel (all), natural and enriched zinc (for ^{61}Cu only)
Product purity	^{60}Cu	~98.8 to ~99.9%
Major impurities		^{61}Cu, ^{55}Co, ^{57}Co
Product purity	^{61}Cu	~99.6% for ^{61}Ni(p,n)^{61}Cu nuclear reaction; >95% for ^{64}Zn(p,α)^{61}Cu nuclear reaction
Major impurities		^{58}Co for ^{61}Ni(p,n)^{61}Cu nuclear reaction; ^{66}Ga, ^{67}Ga, ^{68}Ga for ^{64}Zn(p,α)^{61}Cu nuclear reaction
Product purity	^{64}Cu	~95 to >99%
Major impurities		^{55}Co, ^{56}Co, ^{57}Co, ^{58}Co, ^{57}Ni
Separation method	Ni	Anion exchange chromatography (AG 1-X8 resin) - Target dissolution: (a) HNO_3 or (b) strong HCl - Ni target elution: (a) 0.2 N HCl in 96% methanol or (b) 6N HCl - Co impurity elution: (a) 0.3% HCl in 72% ethanol or (b) 4 N HCl - Copper elution: (a) 0.3 N HCl in 40% ethanol or (b) water
Product separation yield		95%
Target recovery yield		90%
Separation method	Zn	Ion exchange chromatography in series (AG 50W-X8 resin (cation) and AG 1-X8 resin (anion)) - Target dissolution: 10 N HCl - (Cation exchange) Cu and Zn elution: 10 N HCl - (Anion exchange) Cu elution: 2 N HCl - (Anion exchange) Zn target elution: 0.5 N HCl
Product separation yield		—
Target recovery yield		90%

Table 5 Production and purification parameters for ^{55}Co

Radioisotope	^{55}Co
Target material	Natural and enriched nickel
Product purity	92 to >97%
Major impurities	^{57}Co, ^{58}Co, ^{57}Ni
Separation method	Anion exchange chromatography (AG1-X8 resin) - Target dissolution: concentrated HCl - Co elution: 0.4–0.5 N HCl
Product separation yield	>90%
Target recovery yield	94%

keV) coupled with prolonged residence in critical organs which require careful dosimetry studies prior to translation.

Production. ^{52g}Mn is primarily produced using the ^{52}Cr(p,n)^{52g}Mn nuclear reaction.[92,94–96] The reaction takes place within the 20 to 10 MeV beam energy range.[93] The main target material used is natural chromium (isotopic composition: 4.35% ^{50}Cr, 83.79% ^{52}Cr, 9.50% ^{53}Cr, 2.37% ^{54}Cr) which can be loaded on to metal target substrates such as copper[95] and silver[94] *via* electroplating or pressing.[92,94,95] The natural chromium targets may also be a metal disk[92,93] or foil.[96] The primary impurity produced during the reaction was ^{54}Mn ($t_{1/2}$: 312.2 d, 100.0% EC) *via* the ^{54}Cr(p,n)^{54}Mn nuclear reaction,[92,94] however this impurity can be greatly reduced if ^{52}Cr-enriched targets are used. ^{52m}Mn ($t_{1/2}$: 21.1 min, 96.6% β^+, 1.6% EC, 1.8% IT) was also produced[97] from the irradiation, however the radionuclide decays into ^{52g}Mn relatively quickly after its production. When chromium metal disks were bombarded with 16 MeV proton beams, a yield of 9.6 MBq (μA h)$^{-1}$ (*i.e.* 0.26 mCi (μA h)$^{-1}$) was reported at a purity level of 99.55%.[93] For the composite, chromium/silver pressed targets bombarded at the same beam energy, a yield of 5 MBq (μA h)$^{-1}$ (*i.e.* 0.1 mCi (μA h)$^{-1}$) at a purity level of about 95% was reported.[94] When natural chromium foils were irradiated with 12.5 MeV proton beams, a yield of 4.5 MBq (μA h)$^{-1}$ (*i.e.* 0.12 mCi (μA h)$^{-1}$) and a purity exceeding 99.0% was reported by Topping *et al.* (2013).

Product purification. The major method used to isolate manganese from the chromium targets is ion exchange chromatography. There are several different resins that can be used to carry out the isolation procedure. The most frequently used resin was the AG 1-X8 which required dissolution of the bombarded target in 11 to 12 M HCl.[93,96–98] After dissolution, the target solution was passed through the resin which selectively retained the manganese product, and elution was carried out using 0.1 M HCl. The separation efficiency of the process exceeded 97%.[97] Apart from the AG 1-X8 resin, the 50W-X8 resin from Dowex or AG was also used to perform the separation, as discussed by Chaple and Lapi[92] and Wooten *et al.*[95] Methods for recovering the chromium target material have not been discussed, likely because recovery schemes tend not to be feasible when the large natural abundance of ^{52}Cr is considered.

Summary. Table 6 summarizes key production and purification parameters for ^{52g}Mn not mentioned in Table 1.

Niobium: ^{90}Nb

Applications. A relative newcomer PET radionuclide, ^{90}Nb ($t_{1/2}$: 14.6 h, 53.0% β^+, 47.0% EC) is finding increasing consideration as a labelling agent in immunoPET applications due to close agreement between its half-life and the pharmacokinetics of peptides, antibody fragments and antibodies.[99,100] Additionally, ^{90}Nb has a high probability of positron decay at moderate emission energies (β^+ E_{max}: 1.5 MeV), which facilitates high-resolution PET imaging.[101] Protein labelling studies have been carried out as a preliminary step, including ^{90}Nb-labelled monoclonal antibodies rituximab and bevacizumab in high yields.[102–104] ^{90}Nb has also been used to label the peptide derivative DFO-succinyl-(D)Phe1-octreotide.[105] Although easily produced using low-energy cyclotrons, efficient separation methods ensuring quick isolation of ^{90}Nb from bombarded target materials have not yet been established.[99,105]

Production. ^{90}Nb is primarily produced *via* the ^{90}Zr(p,n)^{90}Nb nuclear reaction within the 19 to 7 MeV beam energy range.[99,105] However, ^{90}Nb could also be produced *via* the ^{91}Zr(p,2n)^{90}Nb nuclear reaction when the incident beam energy exceeded 15 MeV.[105] Maximum ^{90}Nb production occurred at a beam energy of 13.5 MeV.[105] The target material for ^{90}Nb production was typically natural zirconium foils (isotopic composition: 51.45% ^{90}Zr, 11.22% ^{91}Zr, 17.15% ^{92}Zr, 17.38% ^{94}Zr, 2.80% ^{96}Zr),[99,101–103,105] although the use of this target produced a significant number of impurities, making it unsuitable for clinical trial applications.[105] The primary impurities produced during the bombardment of natural zirconium were $^{89g/m}$Nb ($t_{1/2}$: 2.0 h, 75.0% β^+, 25.0% EC/66.0 min, 81.0% β^+, 19.0% EC), ^{91m}Nb ($t_{1/2}$: 60.9 d, 96.6% IT, 3.4% EC), ^{92m}Nb ($t_{1/2}$: 10.2 d, 0.1% β^+, 99.9% EC), $^{95g/m}$Nb ($t_{1/2}$: 35.0 d, 100.0% β-/$t_{1/2}$: 3.6 d, 5.6% β-, 94.4% IT), ^{96}Nb ($t_{1/2}$: 23.4 h, 100.0% β-), ^{87}Y ($t_{1/2}$: 79.8 h, 0.2% β^+, 99.8% EC) and ^{89}Zr ($t_{1/2}$: 78.4 h, 22.7.0% β^+, 77.3% EC).[102,105] An alternative production route using ZrO_2 from enriched ^{90}Zr has been proposed by ref. 105, in which case the target preparation involved sedimentation of enriched ZrO_2 powder onto a copper substrate. Production using the $^{90}ZrO_2$ targets had up to two orders of magnitude lower impurity levels. When three, 0.25 mm thick natural zirconium foils were irradiated with a 17.5 MeV proton beam, a ^{90}Nb yield of 145 MBq (μA h)$^{-1}$ (*i.e.* 3.9 mCi (μA h)$^{-1}$) was reported with a purity of 97% at EOB.[102] A yield of 596 MBq (μA h)$^{-1}$ (*i.e.* 16.1 mCi (μA h)$^{-1}$) with purity exceeding 95% was reported following the bombardment of

Table 6 Production and purification parameters for ^{52g}Mn

Radioisotope	^{52g}Mn
Target material	Natural chromium
Product purity	95 to 99.55%
Major impurities	^{54}Mn, ^{52m}Mn
Separation method	Ion exchange chromatography (AG1-X8 resin or other resins) - Target dissolution: 11 N HCl - Mn elution: 0.1 N HCl
Product separation yield	97%
Target recovery yield	n/a

three $^{90}ZrO_2$-on-copper foil targets with an incident proton beam energy of 11.9 MeV, 4 hours after EOB.[105]

Product purification. There are two established methods that have been used to isolate the niobium product from post-bombarded zirconium targets. The first method was described by Radchenko *et al.*[100,103] and required serial ion exchange chromatography separation. Irradiated zirconium targets were first dissolved in 28 M hydrofluoric acid and diluted to 21 M before loading on to the first ion exchange column. Cation exchange was performed by passing the solution through a DOWEX 50 × 8 resin (200–400 mesh) to retain trace metal ion impurities (*i.e.* copper and iron), colloids and undissolved particulate, while allowing the dissolved target material and product to pass through. After washing with concentrated HF, the emerging solution from the cation exchange stage was transferred to the second ion exchange stage. Anion exchange was performed using an AG 1 × 8 resin (200–400 mesh) resin to retain the niobium product. To elute the niobium, a mixture of 1% H_2O_2 in 6 M HCl[101] or 0.1 M oxalic acid[103] was used. If the former was used for elution, the H_2O_2 should be removed by heating the eluate for 5 min at 120 °C. The overall efficiency of the extraction procedure ranged from 93 to 95%.

A second method was described by Radchenko *et al.*,[101,102] which made use of a liquid–liquid extraction procedure. After placing into a small ice-water bath, the bombarded zirconium targets were dissolved in 48% HF (28 M). After complete target dissolution, 10 M HCl and saturated boric acid were added. More than 99% of the niobium product was then partitioned into chloroform using 0.02 M *N*-benzoyl-*N*-phenylhydroxylamine as a phase transfer catalyst. Liquid–liquid extraction was then performed with vigorous shaking for 20 min. After washing the organic phase with a mixture of 9 M HCl and 0.001 M HF and then 9 M HCl, respectively, the niobium product was re-extracted from the organic phase using aqua regia with an extraction rate ranging from 90–95%. To increase the purity of the obtained ^{90}Nb product, the aqueous layer was subsequently passed through an anion exchange resin. The niobium containing solution was evaporated to dryness and the resulting residue was dissolved in a mixture of 0.25 M HCl and 0.1 M oxalic acid. Anion exchange was performed on the residue using a small Aminex A27 column, and the niobium product was eluted using a mixture of 6 M HCl and 0.01 M oxalic acid. The overall efficiency of the extraction procedure ranged from 76 to 81%.

In general, methods for recovering the zirconium target material have not been discussed, likely due to the lack of feasibility of any proposed recovery scheme given the relatively large natural abundance of ^{90}Zr.

Summary. Table 7 summarizes key production and purification parameters for ^{90}Nb not mentioned in Table 1.

Scandium: ^{44g}Sc

Applications. Favorable decay characteristics and the potential availability of a ^{44}Ti/^{44}Sc generator has brought ^{44g}Sc ($t_{1/2}$: 4.0 h, 94.3% β^+, 5.7% EC) into clinical focus over the past decade. Scandium-44 is a trivalent radionuclide that is readily conjugated to peptides and proteins using common macrocyclic chelators such as DOTA and NOTA. This facilitates the growing number of preclinical and clinical PET studies reported,[106–110] and was exemplified by ^{44g}Sc-labelling of PSMA-617 (*i.e.* peptidomimetic inhibitors) as an alternative for ^{68}Ga-labelling.[111] Due to the four-fold longer half-life, dosimetry measurements could be obtained 19 h post-injection to better match the pharmacokinetics of the ^{177}Lu-labelled therapeutic. Additionally, ^{44}Sc forms a true theranostic pairing with ^{47}Sc.[112]

Production. There are many methods that can be used to produce ^{44g}Sc, ranging from the ^{44}Ti/^{44g}Sc generator[62,111] to small medical cyclotrons.[62,110,113,114] With respect to cyclotron production *via* solid targetry, one of the most common production routes is through the ^{44}Ca(p,n)^{44g,m}Sc nuclear reaction. The process involves the use of solid targets formed from natural calcium (isotopic composition: 96.94% ^{40}Ca, 0.65% ^{42}Ca, 0.14% ^{43}Ca, 2.09% ^{44}Ca, >0.01% ^{46}Ca, 0.19% ^{48}Ca) and enriched ^{44}Ca metal,[113] as well as enriched [^{44}Ca]$CaCO_3$ powders.[62,114] The nuclear reaction takes place over beam energies ranging from 18 to 6 MeV, with the reaction cross-section maximums between 13 and 10 MeV.[114] The yield of ^{44g}Sc produced from the bombardment of >94% enriched [^{44}Ca]$CaCO_3$ powders at a beam energy of 11 MeV was 50 MBq (μA h)$^{-1}$ (*i.e.* 1.4 mCi (μA h)$^{-1}$),[114] while that obtained from the bombardment of natural calcium at a beam energy of 15.6 MeV

Table 7 Production and purification parameters for ^{90}Nb

Radioisotope	^{90}Nb
Target material	Natural and enriched zirconium oxide
Product purity	>95 to 97%
Major impurities	$^{89g/m}$Nb, ^{91m}Nb, ^{92m}Nb, $^{95g/m}$Nb, ^{96}Nb, ^{87}Y, ^{89}Zr
Separation method 1	Serial ion exchange chromatography (DOWEX 50 × 8 resin (cation), AG 1 × 8 resin (anion)) - Target dissolution: 28 M HF - (Cation exchange) 1st Nb elution: concentrated HF - (Anion exchange) 2nd Nb elution: 1% H_2O_2 in 6 M HCl
Product separation yield	93 to 95%
Separation method 2	Liquid–liquid extraction - Target dissolution: 48% HF - Extraction solvents: 10 M HCl + saturated boric acid, 0.02 M *N*-benzoyl-*N*-phenylhydroxylamine in $CHCl_3$, aqua regia
Product separation yield	76 to 81%
Target recovery yield	n/a

was 32 MBq $(\mu A\ h)^{-1}$ (*i.e.* 0.9 mCi $(\mu A\ h)^{-1}$) with a purity exceeding 95%.[110] It should be pointed out that targets with high concentrations of ^{44}Ca perform poorly as solid targets due to their low electrical and heat conductivity properties.[110] The primary impurity produced during bombardment was ^{44m}Sc ($t_{1/2}$: 58.6 h, 98.8% IT, 1.2% EC) which has a negligible effect on PET studies when produced in small amounts.[110] ^{44m}Sc has found new use as an *in vivo* generator in various pharmacokinetic studies[62,113] due to its longer half-life and eventual decay into ^{44g}Sc. Other impurities produced during the proton irradiation of ^{44}Ca include ^{47}Sc ($t_{1/2}$: 3.3 d, 100.0% β-) and ^{48}Sc ($t_{1/2}$: 43.7 h, 100.0% β-), which were formed from trace amounts of ^{48}Ca *via* the $^{48}Ca(p,2n)^{47}Sc$ and $^{48}Ca(p,n)^{48}Sc$ nuclear reactions, respectively.[110,114] Small amounts of ^{43}Sc ($t_{1/2}$: 4.0 h, 88.1% β^+, 11.9% EC)[110] and ^{46}Sc ($t_{1/2}$: 83.8 d, 100.0% β-)[62] have also been reported.

Product purification and target recovery. After acid dissolution, the scandium product can be isolated from irradiated calcium targets through column chromatography. However, the specific column and resin used varied with the type of target bombarded. With ^{44}Ca metal, the target was first dissolved in concentrated HCl and then a UTEVA extraction resin was used to retain both the scandium product and the target material.[110] The bulk target material was eluted with the 10 M HCl, while the scandium product was eluted subsequently with water, recovering ~80% of the ^{44g}Sc activity at EOB. When irradiating [^{44}Ca]$CaCO_3$, a chelating ion exchange resin (*i.e.* Chelex 100) was used[114] after target dissolution in 0.1 M HCl. The resin retains both the scandium product and the target material, with the latter eluted first using 0.01 M HCl. The scandium product was removed using 1 M HCl with a separation efficiency exceeding 70%. A target-material recovery stage was further described in the work published by Krajewski *et al.*[114] Briefly, the target-containing effluent was concentrated with ammonia. The new solution was subsequently heated to 170 °C to decompose NH_4Cl formed from the ammonia addition, and to evaporate any remaining water. ^{44}Ca was recovered as ^{44}CaO with a recovery efficiency of 60%, although the authors believed the small batch sizes processed strongly affected the recovery efficiency. Regardless, the addition of a recovery stage was worthwhile given the cost of ^{44}Ca.[62]

Summary. Table 8 summarizes key production and purification parameters for ^{44g}Sc not mentioned in Table 1.

Table 8 Production and purification parameters for ^{44g}Sc

Radioisotope		^{44g}Sc
Target material		Natural and enriched calcium, enriched calcium carbonate
Product purity		>95%
Major impurities		^{44m}Sc, ^{47}Sc, ^{48}Sc, ^{43}Sc, ^{46}Sc
Separation method	1	Ion exchange chromatography (UTEVA extraction resin) - Target dissolution: concentrated HCl - Ca elution: 10 M HCl - Sc elution: water
Product separation yield		80%
Target recovery yield		—
Separation method	2	Ion exchange chromatography (Chelex 100 resin) - Target dissolution: 0.1 M HCl - Sc elution: 0.01 M HCl - Ca elution: 1 M HCl
Product separation yield		70%
Target recovery yield		60%

Technetium: ^{94m}Tc

Applications. The workhorse of nuclear medicine is the SPECT isotope ^{99m}Tc.[115] As a PET surrogate, ^{94m}Tc ($t_{1/2}$: 52 min, 70.2% β^+, 29.8% EC) has seen limited use. Efflux transporter activity has been measured with ^{94m}Tc-sestamibi. The tracer was used in a preclinical multi-drug resistance study involving P-glycoprotein knock-out and wild-type mice, and showed delayed tracer clearance in the liver and kidney of the former group.[116] Other examples include examining cardiac function and estrogen receptor expression.[117,118] A major application of ^{94m}Tc remains the quantitative assessment of novel ^{99m}Tc radiopharmaceuticals through *in vivo* PET studies.[119] The limited adoption of ^{94m}Tc in PET can be attributed to several factors, with the most limiting being the prevalence of the high-energy gamma ray that is released during its decay.[120] Clinical applications using ^{94m}Tc for testing ^{99m}Tc radiopharmaceuticals are also limited by the relatively short half-life of ^{94m}Tc,[120] as well as the poor dosimetry of ^{94m}Tc which is seven-fold less favorable than that of ^{99m}Tc.[121]

Production. ^{94m}Tc can be produced using the $^{94}Mo(p,n)^{94m}Tc$ nuclear reaction on small medical cyclotrons.[11,119–121] The reaction takes place within the 13 to 6 MeV energy range,[11,119] and has been carried out using both natural molybdenum foils (isotopic composition: 14.53% ^{92}Mo, 9.15% ^{94}Mo, 15.84% ^{95}Mo, 16.67% ^{96}Mo, 9.60% ^{97}Mo, 24.39% ^{98}Mo, 9.82% ^{100}Mo) and ^{94}Mo-enriched molybdenum oxide (*i.e.* MoO_3) pellets and powders.[120–122] When using ^{94}Mo-enriched targets for production, the major impurity produced was ^{94g}Tc ($t_{1/2}$: 293 min, 10.5% β^+, 89.5% EC),[119] especially when bombardment was conducted with beam energies equaling or exceeding 13 MeV.[120] When natural molybdenum was used for production, impurities such as $^{95g/m}Tc$ ($t_{1/2}$: 61.0 d, 0.4% β^+, 96.1% EC, 3.9 IT/$t_{1/2}$: 20.0 h, 100.0% EC), $^{96g/m}Tc$ ($t_{1/2}$: 4.3 d, 100.0% EC/$t_{1/2}$: 51.5 min, 98.0% IT, 2.0% EC) and ^{99m}Tc ($t_{1/2}$: 6.0 h, 100.0% IT) were present in addition to ^{94g}Tc.[120–122] Despite the myriad of impurities formed, ^{94m}Tc production from natural molybdenum has been considered suitable for human radiopharmaceutical studies.[120] However, special attention should be given to ^{96m}Tc (which does not emit any imageable gamma rays)[120] and ^{95}Tc,[123] which are both produced in significant amounts and have been shown to increase patient dose. When natural molybdenum foils were bombarded with an 11 MeV proton beam, a saturation yield of 111 MBq $(\mu A\ h)^{-1}$ (*i.e.* 3 mCi $(\mu A\ h)^{-1}$) was reported.[121] However, a theoretical yield of 2000 MBq $(\mu A\ h)^{-1}$ (*i.e.* 54 mCi $(\mu A\ h)^{-1}$) has been calculated for thick targets of enriched ^{94}Mo bombarded with beam energies ranging from 13 to 7 MeV.[120,122]

Product purification and target recovery. The primary method used to separate the technetium product from the metallic or

oxide molybdenum target material was thermochromatographic dry distillation.[120,121] This requires heating of the irradiated targets in moist air,[120] oxygen or helium.[121] For molybdenum oxide targets heated to temperatures below 800 °C, volatile technetium species such as [^{94m}Tc]$HTcO_4$ and [^{94m}Tc]Tc_2O_7 sublime and were transported by the carrier gas until condensation temperatures (*i.e.* 250 to 350 °C) were reached. When heating was carried out at temperatures above 800 °C (*i.e.* 1090 °C (ref. 120)), both the technetium product and molybdenum target material sublimed. The molybdenum condenses first in the 600 to 800 °C temperature range, while the technetium product condenses at the cooler temperatures mentioned above. The condensed technetium product can be dissolved using hot NaOH and purified using a minimized alumina column. The entire separation process required approximately 25 minutes, and had an 80 to 85% product separation efficiency. The molybdenum target material was well isolated and could be easily recovered for immediate reuse with a recovery efficiency exceeding 95%.

Summary. Table 9 summarizes key production and purification parameters for ^{94m}Tc not mentioned in Table 1.

Table 9 Production and purification parameters for ^{94m}Tc

Radioisotope	^{94m}Tc
Target material	Natural molybdenum, enriched molybdenum oxides
Product purity	—
Major impurities	^{94}Tc, $^{95g/m}$Tc, $^{96g/m}$Tc, ^{99m}Tc
Separation method	Thermochromatographic dry distillation (500 to 1090 °C in moist air, O_2 or He; hot NaOH for precipitate dissolution)
Product separation yield	80 to 85%
Target recovery yield	>95%

Titanium: ^{45}Ti

Applications. Favorable decay characteristics has garnered increase consideration of ^{45}Ti ($t_{1/2}$: 3.08 h, 84.8% β^+, 15.2% EC) as a PET imaging agent. These include a reasonable half-life and decaying to a stable daughter isotope, both of which are desirable features for PET radionuclides.[124] Additionally, ^{45}Ti has a high probability of positron decay at a moderate maximum positron energy (β^+ E_{max}: 1040).[92,124] Most positron decay events proceed directly to the ground state, making positron annihilation the primary source of gamma rays in the system.[124,125] These decay characteristics yield images that possess a high resolution.[92] In addition to its favorable decay properties, ^{45}Ti is also available to produce as discussed below. Despite its appeal, research on ^{45}Ti radiolabeled tracers is limited as a result attributed to titanium's complicated chemistry and its high reactivity with oxygen.[92,126] Regardless, a few studies using ^{45}Ti-radiolabelled molecules exist. ^{45}Ti has been used to label human serum albumin, phytate, DTPA and citrate for preclinical studies.[125] A few bioconjugate studies have been completed including protein and peptide targeting vectors. Biodistributions studies in mice using [^{45}Ti]transferrin observed high ^{45}Ti uptake in the spleen and liver[126] indicative of transchelation. Another recent example attached ^{45}Ti to a PSMA-targeted peptidomimetic.[126] In an interesting attempt to develop dual modality probes, chelate free mesoporous silica nanoparticles were labeled with ^{45}Ti for non-invasive *in vivo* quantification.[127]

Production. ^{45}Ti is produced *via* the ^{45}Sc(p,n)^{45}Ti nuclear reaction.[128] The reaction primarily takes place within the 16 to 8 MeV energy range, with a threshold energy of 2.9 MeV.[128] Regardless, a range restricted to 15 to 8 MeV was recommended to reduce the production of isotopic and non-isotopic impurities during bombardment.[124] The primary impurities produced during bombardment were ^{44}Ti ($t_{1/2}$: 59.1 years, 100.0% EC) from the ^{45}Sc(p,2n)^{44}Ti nuclear reaction, and ^{44g}Sc ($t_{1/2}$: 4.0 h, 94.3% β^+, 5.7% EC) from the ^{45}Sc(p,pn)^{44g}Sc and ^{45}Sc(p,d)^{44g}Sc nuclear reactions.[128] The target material was natural scandium (isotopic composition: 100.00% ^{45}Sc) foils.[92,124–126,128] A few values for ^{45}Ti yields have been reported in the literature. Vavere and Welch[126] reported yields of 422 MBq (μA h)$^{-1}$ (*i.e.* 11.4 mCi (μA h)$^{-1}$) after bombarding 0.25 mm thick natural scandium foils with a 14.7 MeV proton beam. However, yields as low as 230 MBq (μA h)$^{-1}$ (*i.e.* 6.2 mCi (μA h)$^{-1}$) for bombardments at 11.8 MeV have been reported.[127]

Product purification. Cation-exchange chromatography has been used to isolate the titanium product from the scandium targets, and the method has been extensively described by Vavere *et al.*[125] and Vavere and Welch.[126] Post-bombarded targets were first dissolved in 6 N HCl, and the final solution was added to a cation exchange column filled with AG 50W-X8 resin (100–200 mesh). ^{45}Ti was then eluted with 6 N HCl, and this eluate was heated in the presence of a nitrogen stream to evaporate the HCl from the final product. Greater than 92% of the eluted ^{45}Ti product was obtained with a radionuclide purity of 99.8%. Methods for recovering the scandium target material have not been discussed as such methods would likely not be feasible due to the naturally high abundance of ^{45}Sc.

Summary. Table 10 summarizes key production and purification parameters for ^{45}Ti not mentioned in Table 1.

Yttrium: ^{86g}Y

Applications. As part of the original theranostic pairing,[129] ^{86g}Y ($t_{1/2}$: 14.7 h, 31.9% β^+, 68.2% EC) is a residualizing radioisotope that has promising applications in radioimmunotherapy as an imaging compliment to its chemically-identical therapeutic counterpart, ^{90}Y. Owing to its well-elucidated chelation chemistry, ^{86g}Y has been used to label several different antibodies, although the produced radiotracers have been limited to use in preclinical studies[1] due to a few limitations. ^{86g}Y decays primarily by electron capture, generating several gamma emissions in the process. This negatively affects imaging quality and necessitates the use of corrections.[130] A second limitation is the accumulation of unbounded ^{86g}Y (due to conjugate dissociation or transchelation) in bone marrow, resulting in acute bone marrow toxicity. However, it should be mentioned that the risk of transchelation for ligands such as DOTA is low given the high thermodynamic and kinetic inertness of Y-DOTA chelates.[131] Various peptides[132,133] and antibodies[134–137] have been radiolabeled with the intention of monitoring radioimmunotherapy. With respect to its utility as

a theranostic pair, the half-life of ^{86g}Y is short compared to ^{90}Y and may limit the flexibility of radioimmunotherapy applications.[1,138] Beyond immunoPET, ^{86}Y has potential for use as a surrogate for gadolinium for non-invasive quantification of MR contrast agents.[139]

Production. ^{86g}Y is primarily produced *via* the ^{86}Sr(p,n)^{86g}Y nuclear reaction, which also produces significant amounts of ^{86m}Y ($t_{1/2}$: 47.4 min, 99.3% IT, 0.4% β^+, 0.3% EC), a shorter half-life impurity which quickly decays into ^{86g}Y.[62] ^{86g}Y has been produced from the bombardment of solid targets made from pressed, enriched $^{86}SrCO_3$ (ref. 140–142) or ^{86}SrO[141] powders using proton beams of energies ranging from 15.1 to 11 MeV.[140,142] Naturally, the yield of ^{86g}Y varied with the solid target material used as well as the specific irradiation conditions employed. When bombardments were carried out using 95.6% enriched $^{86}SrCO_3$ solid target using a 15.1 MeV proton beam, an average ^{86g}Y yield of 48 MBq $(\mu A\ h)^{-1}$ (*i.e.* 1.3 mCi $(\mu A\ h)^{-1}$) with a purity exceeding 99% was obtained.[62,140] Alternatively, bombardments carried out on 96.4% enriched ^{86}SrO targets using a 14.5 MeV proton beam produced much higher ^{86g}Y yields of 166 MBq $(\mu A\ h)^{-1}$ (*i.e.* 4.5 mCi $(\mu A\ h)^{-1}$), with ^{86m}Y (220%), $^{87g/m}$Y ($t_{1/2}$: 79.8 h, 0.2% β^+, 99.8% EC/$t_{1/2}$: 13.3 h, 98.4% IT, 0.8 β^+, 0.8% EC) (0.27%/0.43%) and ^{88}Y ($t_{1/2}$: 106.6 d, 0.2% β^+, 99.8% EC) (0.024%) being the primary impurities.[62,141]

Product purification and target recovery. Multistage-electrolysis and filtration were two primary methods used to extract yttrium from post-bombardment strontium solid targets. The multistage-electrolysis procedure has been reported by Reischl *et al.*[140] and Yoo *et al.*,[141] and first required dissolution of the target material in 2.8 M HNO_3. To displace any oxygen and carbon dioxide dissolved in solution, the solution is sparged with an inert gas (*i.e.* argon) for 10 to 15 min before electrolysis began and continued through two electrolysis stages. The first electrolysis stage was carried out using a platinum plate cathode and anode. Yttrium was deposited on the cathode, followed by transfer to a platinum wire during a second electrolysis stage, where it was later removed and used for downstream labelling procedures. A simpler filtration method required dissolution of the targets in 6 M HCl, followed by the subsequent addition of 1 M NH_4OH.[142] The resulting solution was then filtered under vacuum and washed with water to remove any residual strontium-containing liquid absorbed into the filter paper. Although the filtration-based separation technique was considerably faster than the multistage-electrolysis technique, filtration-based separation suffered from a lower efficiency which affected overall yttrium yields. Multistage-electrolysis boasts separation efficiencies of about 97%, while the separation yield for filtration was about 88%.[62] The strontium remaining in solution after electrolysis and filtration was available to be recovered for reuse. Depending on the chemical form of the strontium, a solution of $(NH_4)_2CO_3$ (ref. 140 and 142) or NH_4OH followed by the addition of saturated ammonium carbonate solution[141] was used to precipitate the strontium in the form of $^{86}SrCO_3$ with a recovery efficiency exceeding 90%. The $^{86}SrCO_3$ can be converted to ^{86}SrO through thermal decomposition if desired.[141]

Summary. Table 11 summarizes key production and purification parameters for ^{86g}Y not mentioned in Table 1.

Zinc: ^{63}Zn

Applications. Zinc is the second most abundant transition metal in the human body being essential to numerous somatic processes, ranging from enzymatic stability to DNA regulation.[143–145] Consequently, zinc dysregulation has been associated with many diseases, such as diabetes, Alzheimer's disease, and various cancers including breast, pancreatic and prostate cancer.[143,145,146] The critical role of zinc homeostasis in addition to its association to numerous diseases makes the development of non-invasive techniques for monitoring fluctuations in somatic zinc levels of great interest.[143,144] Of the many zinc radioisotopes, only three are positron-emitters, with ^{63}Zn ($t_{1/2}$: 38.5 min, 92.7% β^+, 7.3% EC) showing the greatest promise due to its high probability for positron decay and ease of production.[143] For conjugation, zinc only has one oxidation state which makes designing inert chelates much simpler. Despite its attractive properties, ^{63}Zn is limited by its comparatively short half-life, which restricts its viable application to about 2 hours.[143] Regardless, ^{63}Zn radiotracers are thought to be suitable for a variety of short investigative studies such as blood/tissue zinc transport, pancreas and prostate transport kinetics, and blood–brain barrier investigations.[143] A few clinical and preclinical PET studies have used a [^{63}Zn]zinc citrate radiotracer to monitor zinc transport.[144] One preclinical study found that the radiotracer mainly accumulated in the gastrointestinal tract of mice, although a less significant accumulation in the brain of the animals was also reported. A clinical study comparing [^{63}Zn]citrate uptake in brains of Alzheimer's disease patients and age-matched controls found no observed difference in uptake although the clearance of radioactivity was significantly slower in the patient group.[147]

Production. Although several nuclear reactions can be used to produce ^{63}Zn, the only reaction suitable for production using small medical cyclotrons is the ^{63}Cu(p,n)^{63}Zn nuclear reaction.[144] This reaction takes place within the 16 to 5 MeV range using enriched ^{63}Cu as well as natural copper (isotopic composition: 69.17% ^{63}Cu, 30.83% ^{65}Cu). In both cases, ^{63}Zn production was maximized in the 13 to 12 MeV energy range. The primary target material for the reactions were natural copper foils[148] or natural copper that had been electroplated onto a suitable metal substrate such as gold.[146] When a natural copper foil was bombarded with a 16 MeV proton beam, the

Table 10 Production and purification parameters for ^{45}Ti

Radioisotope	^{45}Ti
Target material	Natural scandium
Product purity	>99%
Major impurities	^{44}Ti, ^{44g}Sc
Separation method	Cation exchange chromatography (AG 50W-X8 resin) - Target dissolution: 6 M HCl - Ti elution: 6 M HCl
Product separation yield	>92%
Target recovery yield	n/a

Table 11 Production and purification parameters for ^{86g}Y

Radioisotope		^{86g}Y
Target material		Strontium oxides
Product purity		>99%
Major impurities		^{86m}Y, $^{87g/m}Y$, ^{88}Y
Separation method	1	Multistage electrolysis - Target dissolution: 2.8 M or 4% HNO_3 - Platinum plate cathode and anode - Inert gas environment
Product separation yield		~97%
Separation method	2	Filtration - Target dissolution: 6 M HCl - Y precipitator: 1 M NH_4OH
Product separation yield		~88%
Target recovery yield	>90%	

reported ^{63}Zn yield was 2470 MBq (μA h)$^{-1}$ (*i.e.* 66.8 mCi (μA h)$^{-1}$) with a purity exceeding 99.9%.[148] The primary impurities generated during bombardment were ^{64}Cu ($t_{1/2}$: 12.7 h, 38.5% β^-, 10.8% β^+, 50.7% EC), ^{62}Zn ($t_{1/2}$: 9.2 h, 8.2% β^+, 91.8% EC), and ^{65}Zn ($t_{1/2}$: 243.9 d, 1.4% β^+, 98.6% EC).[144,148] The presence of the ^{65}Zn isotopic impurity is problematic for PET applications due to its long half-life. To limit the production of this impurity, bombardments at beam energies exceeding 11 MeV have been recommended.[148]

Product purification. A method for isolating zinc from the irradiated natural copper targets is described by ref. 148. The natural copper target was first dissolved in concentrated HNO_3 before undergoing cation exchange with an AG 50W-X8 resin. The resin retained the zinc product, which can be eluted using a mixture of 0.05 N HCl and 85% acetone. The eluted zinc was obtained with a separation efficiency of 88.0%. Methods for recovering the copper target material have not been discussed as such methods would likely be impracticable due to the naturally high abundance of ^{63}Cu.

Summary. Table 12 summarizes key production and purification parameters for ^{63}Zn not mentioned in Table 1.

Zirconium: ^{89}Zr

Applications. The well matched half-life of ^{89}Zr ($t_{1/2}$: 78.4 h, 22.7% β^+, 77.3% EC) with the pharmacokinetics of antibodies has led to more than 90 clinical studies, highlighted by the success of the ZEPHIR trial.[4] These ^{89}Zr-labelled antibodies are used to plan and monitor cancer treatments, visualize *in vivo* biodistribution, determine target expression, and conduct radiotherapy dosimetry. With the advancements in its production and labelling technology, ^{89}Zr has been used to label numerous antibodies (*i.e.* HER1-targeted cetuximab, HER2-targeted trastuzumab, VEGF-targeted bevacizumab, CD20-targeted ibritumomab tiuxetan, transforming growth factor-β (TGF-β)-targeted fresolimumab, CD105-targeted TRC105 and PSMA-targeted 7E11) for both clinical and pre-clinical studies.[1] Most of these examples employed desferoxime (DFO) chelator which is less than ideal for zirconium[149] with significant concentrations of unbound ^{89}Zr found with certain radiotracers such as ^{89}Zr-fresolimumab and ^{89}Zr-bevacizumab. This represents a major drawback of ^{89}Zr as free radiometal will accumulate in the bone and may negatively affect bone marrow health.[150,151] Ongoing efforts to develop improved ^{89}Zr chelates may address many of these concerns.[152–154]

Production. Although several nuclear reactions can be used to produce ^{89}Zr, only the $^{89}Y(p,n)^{89}Zr$ reaction can be feasibly carried out on small medical cyclotrons. Natural yttrium (isotopic composition: 100.00% ^{89}Y) targets can be bombarded with beam energies between 14 to 9 MeV, although the actual range for reasonable, high purity production is somewhat narrower.[62] Bombardments with beam energies exceeding 11.6 MeV lead to the production of the long half-life contaminant, ^{88}Y ($t_{1/2}$: 106.6 d, 0.2% β^+, 99.8% EC) formed *via* the $^{89}Y(p,pn)^{88}Y$ reaction,[155] while beam energies greater than 13 MeV resulted in the production of a second long half-life contaminant, ^{88}Zr ($t_{1/2}$: 83.4 d, 100.0% EC) which is inseparable from the final product and is formed *via* the $^{89}Y(p,2n)^{88}Zr$ reaction.[62] Bombardments with beam energies below 10 MeV are not sufficient for ^{89}Zr production.[62] Many different forms of yttrium targets have been investigated to produce ^{89}Zr. Foil and pressed pellet targets were produced entirely from natural yttrium. Alternatively, targets can be composites composed of yttrium or an yttrium oxide (Y_2O_3) layered onto a suitable metal substrate such as copper using sputtering and deposition techniques.[156,157] A high purity yield of 58 MBq (μA h)$^{-1}$ (*i.e.* 1.6 mCi (μA h)$^{-1}$)[64,158] has been reported in the literature for ^{89}Zr production on yttrium metal targets in the aforementioned beam energy range. While the natural abundance of ^{89}Y is monoisotopic it contains trace impurities of iron, titanium, and gadolinium. Proton interactions with those trace elements during bombardment form radionuclide impurities such as ^{48}V ($t_{1/2}$: 16.0 d, 49.9% β^+, 50.1% EC), ^{156}Tb ($t_{1/2}$: 5.3 d, 100.0% EC), ^{65}Zn ($t_{1/2}$: 243.9 d, 1.4% β^+, 98.6% EC) and ^{56}Co ($t_{1/2}$: 77.2 d, 19.7% β^+, 80.3% EC) which negatively affect ^{89}Zr antibody labelling and patient dosimetry.[156]

Product purification. To ensure high zirconium purity, column-based separation methods are generally utilized, with the most common being weak cation exchange.[158,159] The irradiated yttrium targets were dissolved in strong (1 to 3 M) hydrochloric acid, and the solution was passed through a hydroxamate resin column. The hydroxamate column absorbed the zirconium ions in solution and later eluted using 1 M

Table 12 Production and purification parameters for ^{63}Zn

Radioisotope	^{63}Zn
Target material	Natural copper
Product purity	>99.9%
Major impurities	^{64}Cu, ^{62}Zn, ^{63}Zn, ^{65}Zn
Separation method	Cation exchange chromatography (AG 50-X8 resin) - Target dissolution: concentrated HNO_3 - Zn elution: 0.05 N HCl and 85% acetone
Product separation yield	88%
Target recovery yield	n/a

oxalic acid with a separation efficiency exceeding 70%. Depending on the application, a second column-based separation and washing stage could be used to eliminate the oxalic acid from the complex it forms with zirconium since oxalic acid is highly toxic to the human body. When performed, the result was an zirconium product with a final purity exceeding 99.9%.[156–158] Methods for recovering the yttrium target material have not been discussed because recovery of natural Y targets is not practiced due to its economic characteristics *vs.* the purchase of new target material.

Summary. Table 13 summarizes key production and purification parameters for ^{89}Zr not mentioned in Table 1.

Main group elements

Gallium: ^{66}Ga, ^{68}Ga

Applications. Due to its comparatively long half-life, ^{66}Ga ($t_{1/2}$: 9.5 h, 57.0% β^+, 43.0% EC) has received some consideration in the field of PET for longer tracking of radiogallium. However only a few examples of ^{66}Ga PET radiotracers have been reported as the high energy emissions from its decay raises both patient and healthcare personnel safety concerns.[1] In one study, ^{66}Ga was used to label monoclonal antibodies (mAbs) to investigate tumor angiogenesis in animals. The study found that the radiotracer did not clear quickly from the bloodstream of the animals, resulting in moderate amounts of the radiotracer being found in the lungs, liver, heart, kidneys and spleen.[160] A second animal study demonstrated that unbound ^{66}Ga accumulated in the bone and liver, pointing to metabolism or transchelation.[161] On the other hand, ^{68}Ga ($t_{1/2}$: 67.7 min, 88.9% β^+, 11.1% EC) has found extensive use as a small-molecule imaging tool within the last decade.[162–164] ^{68}Ga is particularly advantageous for the labelling of such compounds since its half-life is generally comparable to their pharmacokinetics. Another group of targeting molecules that can be radiolabeled using ^{68}Ga are peptides. These radiotracers are easy and inexpensive to produce and show quick blood clearance and tissue diffusivity. Most of the peptides that have been labelled are analogous to somatostatin, a regulatory protein primarily produced in the nervous and digestive systems. These analogues are able to interact with somatostatin receptors found in normal human tissues (*i.e.* the gastrointestinal tract, kidney, thyroid, spleen, brain, pancreas) and in a variety of malignancies (*i.e.* neuroendocrine tumors, malignant lymphomas, renal cell carcinomas, prostate cancer, breast cancer and small cell lung cancer), thus facilitating PET investigations. ^{68}Ga has also been used to label melanocortin analogues for investigating melanocortin-receptor containing tissues (*i.e.* fibroblasts, leukocytes, keratinocytes, melanocytes and endothelial and antigen-presenting cells), and bombesin analogues for investigating bombesin-receptor containing tissue found in tumors (*i.e.* breast and prostate cancers). It is evident that ^{68}Ga peptide radiotracers have been used in numerous preclinical and clinical studies,[165] including nearly 400 clinical investigations. The promising potential of ^{68}Ga radiopharmaceuticals have found clinical utility through successful imaging of PSMA, somatostatin receptors, and FAPI.[163,164,166]

Production. ^{66}Ga can be produced from the bombardment of both natural zinc (isotopic composition: 49.17% ^{64}Zn, 27.73% ^{66}Zn, 4.04% ^{67}Zn, 18.45% ^{68}Zn, 0.61% ^{70}Zn) and ^{66}Zn-enriched foils,[167] or after electroplating onto gold or silver substrates.[160] The radionuclide is primarily produced *via* the ^{66}Zn(p,n)^{66}Ga nuclear reaction at a minimum beam energy of 6 MeV,[161] but irradiations are typically carried out at much higher energies (*i.e.* such as 9.8 MeV,[167] 13 MeV,[160] 14.5 MeV (ref. 167) and 15 MeV (ref. 161)). Yields of 511 MBq (μA h)$^{-1}$ (*i.e.* 13.8 mCi (μA h)$^{-1}$) with a purity of 99.96% have been achieved from the 14.5 MeV bombardment of 98.9% enriched ^{66}Zn targets[167] although higher yields of 700 MBq (μA h)$^{-1}$ (*i.e.* 18.9 mCi (μA h)$^{-1}$) have been reported elsewhere.[64] The primary impurity produced during irradiation was ^{67}Ga ($t_{1/2}$: 3.3 d, 100.0% EC).[161,167]

While ^{68}Ga has traditionally been produced with ^{68}Ge/^{68}Ga generators producing 1850 MBq and 3700 MBq of ^{68}Ga, cyclotrons have alternatively been used for its production *via* the proton bombardment of ^{68}Zn-enriched targets. Recent progress using liquid targets has demonstrated modest production yields above ^{68}Ge/^{68}Ga generators. However solid targets show significant potential for much higher capacity production.[168] Solid targets may be foils or zinc-coated metal backings (*i.e.* aluminum, gold or silver) that are generally prepared *via* electroplating or sputtering.[169–171] The primary reaction governing the production of ^{68}Ga is the ^{68}Zn(p,n)^{68}Ga nuclear reaction, which takes place within the 14 to 11 MeV beam energy range.[62] Researchers have reported approximate yields of 1240 MBq (μA h)$^{-1}$ (*i.e.* 33.5 mCi (μA h)$^{-1}$) from the bombardment of natural zinc targets at a beam energy of 12.5 MeV,[171] and yields of 1380 MBq (μA h)$^{-1}$ (*i.e.* 37.3 mCi (μA h)$^{-1}$) for the bombardment of enriched >99% ^{68}Zn electroplated silver targets with a beam energy of 12.5 MeV.[169] A novel enriched zinc target design (backed with silver) irradiated at 13 MeV demonstrated a final yield of 1213 MBq (μA h)$^{-1}$ (*i.e.* 32.8 mCi (μA h)$^{-1}$) at end of separation (EOS) with a purity exceeding 99%.[172] The major impurities produced from the reaction were ^{66}Ga ($t_{1/2}$: 9.5 h, 57.0% β^+, 43.0% EC) and ^{67}Ga ($t_{1/2}$: 3.3 d, 100.0% EC), and they are inseparable from the desired isotope.[62] Measures can be taken to reduce $^{66/67}$Ga production during target irradiation including: (1) reduce the amounts of ^{66}Zn and ^{67}Zn in the targets by using highly enriched ^{68}Zn to limit the ^{66}Zn(p,n)^{66}Ga and ^{67}Zn(p,n)^{67}Ga nuclear reactions, and (2) limit the maximum

Table 13 Production and purification parameters for ^{89}Zr

Radioisotope	^{89}Zr
Target material	Natural yttrium and its oxide
Product purity	>99.9%
Major impurities	^{88}Y, ^{88}Zr, ^{48}V, ^{156}Tb, ^{65}Zn, ^{56}Co
Separation method	Cation exchange chromatography (hydroxamate resin) - Target dissolution: 1 to 3 M HCl - Zr elution: 1 M oxalic acid
Product separation yield	70%
Target recovery yield	n/a

beam energy to 12 MeV to reduce the ^{68}Zn(p,2n)^{67}Ga nuclear reaction[62] respectively.[169]

Product purification and target recovery. Gallium can be extracted from the zinc targets through two major methods. The first method made use of cation exchange chromatography where irradiated targets were dissolved in 10 to 12 M HCl and passed through a cation exchange resin, such as the AG 50W-X8 or AG 50W-X2, which retained both the zinc target material and gallium product. The zinc target material was then eluted using 10 M HCl, and was recovered with efficiencies ranging from 76 to 80%. The gallium product was subsequently eluted with 4 M HCl with an overall separation efficiency as high as 90%.[160,167,170] To increase the purity of the obtained gallium, a washing stage using 7 N HCl was carried out immediately before eluting the gallium product.[170] Alternatively, this procedure was carried out in a fully automated way using commercially available modules with separation efficiencies up to 80%.[169,171–173] Unreacted zinc target material was recovered from the 10 M HCl solution through electrolysis using a voltage of 5 V and a current of 1 A with efficiencies exceeding 76%.[169]

The second method for isolating gallium is liquid–liquid extraction. Preparation steps for this procedure involved dissolving the irradiated zinc targets in 12 M acid and diluting the resulting solution to 7 M with water. The dissolution was then subjected to a series of extraction and back-extraction stages using various solvents (*i.e.* diisopropyl ether, 7 M HCl and water) until gallium was obtained with the desired purity.[167] Maximum separation efficiency for the gallium product was 79% and the recovery efficiency for the zinc target material exceeded 99%.

Summary. Table 14 summarizes key production and purification parameters for ^{66}Ga and ^{68}Ga not mentioned in Table 1.

Arsenic: ^{72}As

Applications. ^{72}As ($t_{1/2}$: 26.0 h, 87.8% β^+, 12.2% EC) is considered a promising PET radionuclide for several reasons including its long nuclear half-life which permits the radiolabeling of biomolecules with longer biological half-lives.[174,175] The resulting radiotracers can be used in several extended biochemical and physiological process studies such as immunoimaging and receptor mapping. A second favorable characteristic arises from the unique soft Lewis acid properties of arsenic to covalently bond to thiol (or sulfhydryl) groups.[1,174,175] Theoretically, this allows arsenic's radioisotopes to directly label numerous biomolecules with little to no chemical modification.[1,175] Several radioarsenic labeled antibodies and nanoparticles have been reported, although none have entered clinical use.[176–178] Finally, the positron emitting ^{72}As provides a matched pair with ^{77}As ($t_{1/2}$: 38.8 h, 100% β^-) which will behave identically *in vivo* for imaging and radiotherapy, respectively.[179] The theranostic advantage of the pairing makes up for the poor image resolution resulting from arsenic's large positron range (*i.e.* 3.6 mm in soft tissue).[58] Despite its favorable qualities however, research on the PET applications of ^{72}As has been slow as a result of the limited supply of isotopically-enriched germanium, the primary material for the production of various arsenic radioisotopes,[1,175] although selenium has been used on occasion.[180] The limited supply of isotopically-enriched germanium increases target costs which translates into an overall increase in ^{72}As production costs.[175]

Production. ^{72}As can be produced using a ^{72}Se/^{72}As generator, or using a solid target cyclotron.[1] With respect to the latter, ^{72}As can be produced using a variety of nuclear reactions such as ^{72}Ge(p,n)^{72}As, ^{73}Ge(p,2n)^{72}As, ^{74}Ge(p,3n)^{72}As and ^{76}Se(p,x)^{72}As.[180,181] Of the listed reactions, the most commonly used was the ^{72}Ge(p,n)^{72}As nuclear reaction which took place within the 18 to 8 MeV range,[174] noting that ^{72}As production at beam energies exceeding 15 MeV contained a greater number of impurities in the final product.[174] The targets used for ^{72}As production were typically ^{72}Ge-enriched germanium disks[178] and ^{72}Ge-enriched germanium oxide that had been electroplated onto substrates made of copper[174] and niobium.[175] Additionally, natural germanium oxide[174] or natural germanium (isotopic composition: 20.57% ^{70}Ge, 27.45% ^{72}Ge, 7.75% ^{73}Ge, 36.50% ^{74}Ge, 7.73% ^{76}Ge) foil[182] have also been used to produce

Table 14 Production and purification parameters for ^{66}Ga and ^{68}Ga

Radioisotope		^{66}Ga, ^{68}Ga
Target material	^{66}Ga	Natural and enriched zinc
Product purity		>99.9%
Major impurities		^{67}Ga
Target material	^{68}Ga	Enriched zinc
Product purity		>99%
Major impurities		^{66}Ga, ^{67}Ga
Separation method	1	Cation exchange chromatography (AG 50W-X8 and AG 50W-X2 resins) - Target dissolution: 10 to 12 M HCl - Zn elution: 10 M HCl - Ga elution: 4 M HCl
Product separation yield		90%
Target recovery yield		76 to 80%
Separation method	2	Liquid–liquid extraction - Target dissolution: 12 M HCl - Extraction solvents: Diisopropyl ether, 7 M HCl and water
Product separation yield		79%
Target recovery yield		>99%

^{72}As in other studies. The primary impurities produced during bombardment were ^{71}As ($t_{1/2}$: 65.3 h, 28.3% β^+, 71.7% EC), ^{74}As ($t_{1/2}$: 17.8 d, 34.0% β^-, 29.0% β^+, 37.09% EC), ^{76}As ($t_{1/2}$: 26.2 h, 100.0% β^-),^{69}Ge($t_{1/2}$: 39.1 h, 24.0% β^+, 76.0% EC) and ^{67}Ga ($t_{1/2}$: 3.3 d, 100.0% EC) (175,178,182). The ^{72}As production yield for >96% enriched germanium oxide electroplated onto a niobium substrate and bombarded with 16.1 MeV protons was 90 MBq $(\mu A\ h)^{-1}$ (*i.e.* 2.4 mCi $(\mu A\ h)^{-1}$), with purity exceeding 99%.[178] The theoretical ^{72}As yield for natural germanium oxide electroplated onto a copper substrate and bombarded with a proton beam energy of 15 MeV to 8 MeV was 60 MBq $(\mu A\ h)^{-1}$ (*i.e.* 1.6 mCi $(\mu A\ h)^{-1}$).[174]

Product purification and target recovery. Methods for isolating arsenic from the germanium targets have been described extensively in Enferadi *et al.*,[174] Ellison *et al.*[175,178] and Guin *et al.*[183] In general, the methods required dissolution of the germanium targets using solutions of 6 M NaOH or hot aqua regia, followed by the addition of 6 to 10 N HCl. The addition of the HCl was necessary to convert the germanium metal to $GeCl_4$, which is significantly more volatile than the metallic arsenic product. Thirty percent hydrogen peroxide was then added to oxidize the arsenic to the As(v) state. The final dissolution was evaporated to near dryness, after which distillation was performed on the resulting residue. About 97% of the ^{72}As was left behind as residue from the distillation, and then further purified through ion exchange chromatography after dissolution in 10 M HCl. Anion exchange was carried out by passing the arsenic solution through a Bio-Rad AG 1 × 8 resin (200–400 mesh), which retained the arsenic product as well as any residual germanium and gallium impurities. The arsenic could be collected by eluting with 10 M HCl, and the procedure had a separation efficiency of 93%, resulting in an overall As(v) separation efficiency of about 90%. However, if it is desirous to have the arsenic in the As(III) state instead of its As(v) state, SPE can be carried out subsequently. The SPE procedure had an efficiency of 57% and after its application, the overall separation efficiency of the As(III) product was 51%. Recovery of the germanium target material could be achieved by treating the acidic condensate from the dissolution stage with 6 M NaOH. This neutralized the condensate, and converted $GeCl_4$ to GeO which could be easily reduced to metallic germanium when sufficiently heated. The overall recovery efficiency reported by Ellison *et al.*[178] was about 60%, however it should be emphasized that higher recovery efficiencies could be achieved if the recovery process was optimized.

Summary. Table 15 summarizes key production and purification parameters for ^{72}As not mentioned in Table 1.

Table 15 Production and purification parameters for ^{72}As

Radioisotope	^{72}As
Target material	Natural and enriched germanium and their oxides
Product purity	>99%
Major impurities	^{71}As, ^{74}As, ^{76}As, ^{67}Ga, ^{69}Ge
Separation method	Distillation, Anion exchange chromatography and SPE - (Distillation) target dissolution: 6 M NaOH or hot aqua regia $^+$ 6 to 10 N HCl $^+$ 30% H_2O_2 - (Chromatography) target distillation: 10 M HCl - As elution: 10 M HCl
Product separation yield	>90% As(v), ~51% As(III)
Target recovery yield	~60%

Conclusion

Given the surge in clinical use and interest in several metallic radioisotopes, solid target systems for small (≤24 MeV) medical cyclotrons are rapidly evolving to enable large-scale production with consistent yield, composition and quality. With this, many factors need to be considered when choosing to develop in-house radiometal production capabilities, including (i) the variability in medical cyclotron design (*i.e.* beam energy, current and machine configuration); (ii) target isotope availability; (iii) quality/quantity variations when compared to alternative, non-cyclotron production routes, and (iv) the intended application of the radioisotope. While many of the metallic radioisotopes discussed herein are being developed as imaging agents unto themselves, several have the potential to be theragnostic partners to a range of chemically diverse therapeutic radioisotopes, and require considerations in chemical compatibility and physical/biological half-life. Of those diagnostic radioisotopes with theragnostic applications, the community will likely see near-term adoption of cyclotron-produced ^{68}Ga and ^{89}Zr, and a resurgence of interest in ^{64}Cu. Radioisotopes with element-identical theragnostic application such as ^{86}Y, ^{44}Sc and ^{124}I may encounter increases in use as long as their production and/or recycling methodologies can be sufficiently optimized. Yet others, such as cyclotron-produced ^{99m}Tc, may emerge as important enablers for those regions in which supply *via* non-cyclotron-based alternatives remain problematic.

Nomenclature and units

α	Alpha particle
β^-	Beta emission
β^+	Positron emission
d	Days
EC	Electron capture
E_{max}	The endpoint energy (*i.e.* maximum energy) of an emitted positron
EOB	End of bombardment
h	Hours
IT	Isomeric transition
keV	Kiloelectron volts
MBq	Megabecquerels
MeV	Megaelectron volts
μA	Microamperes
mCi	Millicuries
min	Minutes
M	Molar (*i.e.* mols of acid per liter)

n	Neutron
N	Normal (*i.e.* moles of dissociated H^+ ions per liter)
°C	Degrees celsius
PET	Positron emission tomography
p	Positron
SPECT	Single photon computed tomography
SPE	Solid phase extraction
$t_{1/2}$	Half-life
γ	Gamma ray

Conflicts of interest

There are no conflicts of interest to declare.

References

1 Y. Zhou, K. E. Baidoo and M. W. Brechbiel, Mapping Biological Behaviors by Application of Longer-Lived Positron Emitting Radionuclides, *Adv. Drug Delivery Rev.*, 2013, **65**(8), 1098–1111.
2 A. Boschi, P. Martini, V. Costa, A. Pagnoni and L. Uccelli, Interdisciplinary tasks in the cyclotron production of radiometals for medical applications - The case of ^{47}Sc as example, *Molecules*, 2019, **24**(3), 444.
3 S. Reddy and M. Robinson, ImmunoPET In Cancer Models, *Semin. Nucl. Med.*, 2010, **40**(3), 182–189.
4 E. Boros and J. Holland, Chemical aspects of metal ion chelation in the synthesis and application antibody-based radiotracers, *J. Labelled Compd. Radiopharm.*, 2018, **61**(9), 652–671.
5 G. Stöcklin and V. W. Pike, *Radiopharmaceuticals for Positron Emission Tomography-Methodological Aspects*, Springer Science & Business Media, Vol. 24, 1993.
6 M. Sajjad and R. M. Lambrecht, Cyclotron targetry for medical radioisotope production, *Nucl. Instrum. Methods Phys. Res., Sect. B*, 1989, **40**, 11001104.
7 H. F. Valdovinos, S. Graves, P. Ellison, T. Barnhart and R. J. Nickles, Earth, air, fire and water: A targetry quartet, *AIP Conf. Proc.*, 2017, 1845.
8 S. M. Qaim, Target development for medical radioisotope production at a cyclotron, *Nucl. Instrum. Methods Phys. Res.*, 1989, **282**(1), 289–295.
9 International Atomic Energy Agency, *Cyclotron produced radionuclides: physical characteristics and production methods* International Atomic Energy Agency, Vienna, Austria, 2009.
10 C. J. Anderson and R. Ferdani, Copper-64 radiopharmaceuticals for PET imaging of cancer: Advances in preclinical and clinical research, *Cancer Biother.Radiopharm.*, 2009, **24**(4), 379–393.
11 M. Fassbender, A. F. Novgorodov, F. Rösch and S. M. Qaim, Excitation Functions of ^{93}Nb(3He,xn)^{93m,g,94m,g,95m,g}Tc-Processes from Threshold up to 35 MeV: Possibility of Production of ^{94m}Tc in High Radiochemical Purity using a Thermochromatographic Separation Technique, *Radiochim. Acta*, 1994, **65**(4), 215–222.
12 H. Büyükuslu, A. Kaplan, G. Yıldırım, A. Aydin, E. Tel and M. Bölükdemir, Production cross sections of medical 110,111 In radionuclides, *Kerntechnik*, 2010, **73**(3), 103–108.
13 T. Kostelnik and C. Orvig, Radioactive main group and rare earth metals for imaging and therapy, *Chem. Rev.*, 2018, **119**(2), 902–956.
14 A. Rahman and A. Awal, Production of ^{149}Tb, ^{152}Tb, ^{155}Tb and ^{161}Tb from gadolinium using different light-particle beams, *J. Radioanal. Nucl. Chem.*, 2020, **323**(2), 731–740.
15 A. Klein, F. Rösch and S. Qaim, Investigation of ^{50}Cr(d,n)^{51}Mn and natCr(p, x)^{51}Mn processes with respect to the production of the positron emitter ^{51}Mn, *Radiochim. Acta*, 2000, **88**(5), 253–264.
16 E. Boros and A. Packard, Radioactive transition metals for imaging and therapy, *Chem. Rev.*, 2018, **119**(2), 870–901.
17 A. H. Asad, S. V. Smith, S. Chan, C. M. Jeffery, L. Morandeau and R. I. Price, Cyclotron production of ^{61}Cu using natural Zn & enriched ^{64}Zn targets, in *AIP Conference Proceedings*, 2012, pp. 91–5.
18 T. Z. Wong, J. L. Lacy, N. A. Petry, T. C. Hawk, T. A. Sporn, M. W. Dewhirst, *et al.*, PET of hypoxia and perfusion with ^{62}Cu-ATSM and ^{62}Cu-PTSM using a ^{62}Zn/^{62}Cu generator, *Am. J. Roentgenol.*, 2008, **190**(2), 427–432.
19 E. Aluicio-Sarduy, N. Thiele, K. Martin, B. Vaughn, J. Devaraj, A. Olson, *et al.*, Establishing radiolanthanum chemistry for targeted nuclear medicine applications, *Chemistry*, 2020, **26**(6), 1238.
20 E. Aluicio-Sarduy, T. Barnhart, J. Weichert, R. Hernandez and J. Engle, Cyclotron produced ^{132}La as a PET imaging surrogate of therapeutic ^{225}Ac, *J. Nucl. Med.*, 2021, **62**(7), 1012–1015.
21 E. Boros and A. B. Packard, Radioactive Transition Metals for Imaging and Therapy, *Chem. Rev.*, 2018, **119**(2), 870–901.
22 E. Aluicio-Sarduy, P. Ellison, T. Barnhart, W. Cai, R. Nickles and J. Engle, PET radiometals for antibody labeling, *J. Labelled Compd. Radiopharm.*, 2018, **61**(9), 636–651.
23 H. Coenen and J. Ermert, Expanding PET-applications in life sciences with positron emitters beyond fluorine-18, *Nucl. Med. Biol.*, 2021, **92**, 241–269.
24 H. Coenen, M. Harmand, G. Kloster and G. Stöcklin, 15-(p-[^{75}Br] bromophenyl) pentadecanoic Acid: Pharmacokinetics and Potential as Heart Agent, *J. Nucl. Med.*, 1981, **22**(10), 891–896.
25 O. De Jesus, G. Van Hoffaert, D. Glock, L. Goldber and A. Friedman, Synthesis of a radiobrominated analog of SCH 23390, a selfctive dopamine D1/DA1 antagonist, *J. Labelled Compd. Radiopharm.*, 1986, **23**(9), 919–925.
26 S. Moerlein and G. Stoecklin, Synthesis of high specific activity [^{75}Br]-and [^{77}Br] Bromperidol and tissue distribution studies in the rat. Journal of medicinal chemistry, *J. Med. Chem.*, 1985, **28**(9), 1319–1324.
27 S. Moerlein, P. Laufer, G. Stöcklin, G. Pawlik, K. Wienhard and W. Heiss, Evaluation of ^{75}Br-labelled butyrophenone neuroleptics for imaging cerebral dopaminergic receptor areas using positron emission tomography, *Eur. J. Nucl. Med.*, 1986, **12**(4), 211–216.

28 J. Rice, N. Hussain and E. Lavoie, Synthesis of [methoxy-^{14}C] eugenol, *J. Labelled Compd. Radiopharm.*, 1987, **24**(9), 1043–1049.

29 G. Kloster, P. Laufer, W. Wutz and G. Stöcklin, ^{75,77}Br-and 123 I-analogues of D-glucose as potential tracers for glucose utilisation in heart and brain, *Eur. J. Nucl. Med.*, 1983, **8**(6), 237–241.

30 D. J. Rowland, T. J. McCarthy and M. J. Welch, Radiobromine for imaging and therapy, in *Handbook of Radiopharmaceuticals: Radiochemistry and Applications*, 2002, pp. 441–465.

31 P. McQuade, D. J. Rowland, J. S. Lewis and M. J. Welch, Positron-Emitting Isotopes Produced on Biomedical Cyclotrons, *Curr. Med. Chem.*, 2005, **12**(7), 807–818.

32 M. Kassiou, C. Loc'h, M. Bottlaender, K. Mardon, M. Ottaviani, C. Coulon, *et al.*, (+)-[^{76}Br] A-69024: a non-benzazepine radioligand for studies of dopamine D1 receptors using PET, *Nucl. Med. Biol.*, 2002, **29**(3), 295–302.

33 C. Foged, C. Halldin, C. Loc'h, B. Mazière, P. Karlsson, M. Mazière, *et al.*, ^{11}C-and ^{76}Br-labelled NNC 22-0010, selective dopamine D1 receptor radioligands for PET, *Nucl. Med. Biol.*, 1996, **23**(6), 837–844.

34 C. Lundkvist, C. Loc'h, C. Halldin, M. Bottlaender, M. Ottaviani, C. Coulon, *et al.*, Characterization of bromine-76-labelled 5-bromo-6-nitroquipazine for PET studies of the serotonin transporter, *Nucl. Med. Biol.*, 1999, **26**(5), 501–507.

35 L. Lang, W. Li, H. Jia, D. Fang, S. Zhang, X. Sun, *et al.*, New methods for labeling RGD peptides with bromine-76, *Theranostics*, 2011, **1**, 341.

36 S. Cho, L. Ravasi, L. Szajek, J. Seidel, M. Green, H. Fine, *et al.*, Evaluation of ^{76}Br-FBAU as a PET reporter probe for HSV1-tk gene expression imaging using mouse models of human glioma, *J. Nucl. Med.*, 2005, **46**(11), 1923–1930.

37 S. Watanabe, H. Hanaoka, J. Liang, Y. Iida, K. Endo and N. Ishioka, PET Imaging of Norepinephrine Transporter–Expressing Tumors Using ^{76}Br-meta-Bromobenzylguanidine, *J. Nucl. Med.*, 2010, **51**(9), 1472–1479.

38 R. Rossin, D. Berndorff, M. Friebe, L. M. Dinkelborg and M. J. Welch, Small-animal PET of tumor angiogenesis using a ^{76}Br-labeled human recombinant antibody fragment to the ED-B domain of fibronectin, *J. Nucl. Med.*, 2007, **48**(7), 1172–1179.

39 N. Vaiseman, G. Koren and P. Pencharz, Pharmacokinetics of oral and intravenous bromide in normal volunteers, *J. Toxicol. Clin. Toxicol.*, 1986, **24**(5), 403–413.

40 C. Lang, D. Habs, K. Parodi and P. Thirolf, Sub-millimeter nuclear medical imaging with high sensitivity in positron emission tomography using β^+ γ coincidences, *J. Instrum.*, 2014, **9**(1), P01008.

41 M. Sitarz, J. Cussonneau, T. Matulewicz and F. Haddad, Radionuclide candidates for β^+ γ coincidence PET: an overview, *Appl. Radiat. Isot.*, 2020, **155**, 108898.

42 D. Wilbur and M. Adam, Radiobromine and radioiodine for medical applications, *Radiochim. Acta*, 2019, **107**(9–11), 1033–1063.

43 *Progress in Radiopharmacy. Progress in Radiopharmacy*. ed. P Cox, S Mather, C Sampson and C Lazarus, Springer Science & Business Media; 2012.

44 Z. Kovács, G. Blessing, S. M. Qaim and G. Stöcklin, Production of ^{75}Br via the ^{76}Se(p,2n)^{75}Br reaction at a compact cyclotron, *Int. J. Appl. Radiat. Isot.*, 1985, **36**(8), 635–642.

45 S. M. Qaim, Recent developments in the production of ^{18}F, ^{75,76,77}Br and ^{123}I, *Int. J. Radiat. Appl. Instrum. Appl. Radiat. Isot.*, 1986, **37**(8), 803–810.

46 D. J. Schlyer, Production of Radionuclides in Acclerators, in *Handbook of radiopharmaceuticals, radiochemistry and applications*, 2003. pp. 1–70.

47 K. Breunig, I. Spahn, S. Spellerberg and H. H. Coenen, Production of no-carrier-added radiobromine: New nickel selenide target and optimized separation by dry distillation, *Radiochim. Acta*, 2015, **103**(5), 397–402.

48 V. Tolmachev, A. Lövqvist, L. Einarsson, J. Schultz and H. Lundqvist, Production of ^{76}Br by a low-energy cyclotron, *Appl. Radiat. Isot.*, 1998, **49**(12), 1537–1540.

49 A. Bruskin, I. Sivaev, M. Persson, H. Lundqvist, J. Carlssona, S. Sjoberg, *et al.*, Radiobromination of monoclonal antibody using potassium [^{76}Br](4 isothiocyanatobenzyl-ammonio)-bromo-decahydro-closo-dodecaborate (Bromo-DABI), *Nucl. Med. Biol.*, 2004, **31**(2), 205–211.

50 S. Mahajan and C. Divgi, The role of iodine-124 positron emission tomography in molecular imaging, *Clin. Transl. Imaging*, 2016, **4**(4), 297–306.

51 J. A. O'Donoghue, P. M. Smith-Jones, J. L. Humm, S. Ruan, D. A. Pryma, A. A. Jungbluth, *et al.*, ^{124}I-huA33 antibody uptake is driven by A33 antigen concentration in tissues from colorectal cancer patients imaged by immuno-PET, *J. Nucl. Med.*, 2011, **52**(12), 1878–1885.

52 I. Verel, G. W. M. Visser, O. C. Boerman, J. E. M. Van Eerd, R. Finn, R. Boellaard, *et al.*, Long-lived positron emitters zirconium-89 and iodine-124 for scouting of therapeutic radioimmunoconjugates with PET, *Cancer Biother.Radiopharm.*, 2003, **18**(4), 655–661.

53 G. C. Jayson, J. Zweit, A. Jackson, C. Mulatero, P. Julyan, M. Ranson, *et al.*, Molecular imaging and biological evaluation of HuMV833 anti-VEGF antibody: Implications for trial design of antiangiogenic antibodies, *J. Natl. Cancer Inst.*, 2002, **94**(19), 1484–1493.

54 A. M. S. Braghirolli, W. Waissmann, J. B. Da Silva and G. R. Dos Santos, Production of iodine-124 and its applications in nuclear medicine, *Appl. Radiat. Isot.*, 2014, **90**, 138–148.

55 H. Coenen, K. Dutschka, S. Müller, L. Geworski, J. Farahati and C. Reiners, Nca radiosynthesis of [^{123,124} I] β-CIT, plasma analysis and pharmacokinetic studies with SPECT and PET, *Nucl. Med. Biol.*, 1995, **22**(8), 977–984.

56 C. Zechmann, A. Afshar-Oromieh, T. Armor, J. Stubbs, W. Mier, B. Hadaschik, *et al.*, Radiation dosimetry and first therapy results with a $^{124\ I/131}$I-labeled small molecule (MIP-1095) targeting PSMA for prostate cancer therapy, *Eur. J. Nucl. Med. Mol. Imag.*, 2014, **41**(7), 1280–1292.

57 C. Foss, D. Plyku, A. Ordonez, J. Sanchez-Bautista, H. Rosenthal, I. Minn, *et al.*, Biodistribution and radiation dosimetry of ^{124}I-DPA-713, a PET radiotracer for macrophage-associated inflammation, *J. Nucl. Med.*, 2018, **59**(11), 1751–1756.

58 L. Carter, A. Kesner, E. Pratt, V. Sanders, A. Massicano, C. Cutler, *et al.*, The impact of positron range on PET resolution, evaluated with phantoms and PHITS Monte Carlo simulations for conventional and non-conventional radionuclides, *Mol. Imag. Biol.*, 2020, **22**(1), 73–84.

59 N. Shah, H. Herzog, C. Weirich, L. Tellmann, J. Kaffanke, L. Caldeira, *et al.*, Effects of magnetic fields of up to 9.4 T on resolution and contrast of PET images as measured with an MR-BrainPET, *PLoS One*, 2014, **4**, e95250.

60 S. D. Wilbur, S. W. Hadley, M. D. Hylarides, P. G. Abrams, P. A. Beaumier, A. C. Morgan, *et al.*, Development of a stable radioiodinating reagent to label monoclonal antibodies for radiotherapy of cancer, *J. Nucl. Med.*, 1989, **30**(2), 216–226.

61 M. Berman, L. Braverman, J. Burke, L. De Groot, K. McCormack, T. Oddie, *et al.*, Summary of Current Radiation Dose Estimates to Humans from ^{123}I, ^{124}I, ^{125}I, ^{126}I, ^{130}I, ^{131}I, and ^{132}I as Sodium Iodide, *J. Nucl. Med.*, 1975, **16**(12), 1214–1217.

62 M. A. Synowiecki, L. R. Perk and J. F. W. Nijsen, Production of novel diagnostic radionuclides in small medical cyclotrons, *EJNMMI Radiopharm. Chem*, 2018, **3**(1), 3.

63 L. Koehler, K. Gagnon, S. McQuarrie and F. Wuest, Iodine-124: A promising positron emitter for organic PET chemistry, *Molecules*, 2010, **15**(4), 2686–2718.

64 S. M. Qaim, Nuclear data for production and medical application of radionuclides: Present status and future needs, *Nucl. Med. Biol.*, 2017, **44**, 31–49.

65 D. W. McCarthy, L. A. Bass, P. D. Cutler, R. E. Shefer, R. E. Klinkowstein, P. Herrero, *et al.*, High purity production and potential applications of copper-60 and copper-61, *Nucl. Med. Biol.*, 1999, **26**(4), 351–358.

66 S. Lapi, J. Lewis and F. Dehdashti, Evaluation of hypoxia with copper-labeled diacetyl-bis (N-methylthiosemicarbazone), *Semin. Nucl. Med.*, 2015, **45**(2), 177–185.

67 M. Conti and E. Lars, Physics of pure and non-pure positron emitters for PET: a review and a discussion, *EJNMMI Phys*, 2016, **3**(1), 1–7.

68 W. Ping Li, L. A. Meyer, D. A. Capretto, C. D. Sherman and C. J. Anderson, Receptor-binding, biodistribution, and metabolism studies of ^{64}Cu-DOTA-cetuximab, a PET-imaging agent for epidermal growth-factor receptor-positive tumors, *Cancer Biother.Radiopharm.*, 2008, **23**(2), 158–171.

69 M. Lewis, C. Boswell, R. Laforest, T. Buettner, D. Ye, J. Connett, *et al.*, Conjugation of monoclonal antibodies with TETA using activated esters: biological comparison of ^{64}Cu-TETA-1A3 with ^{64}Cu-BAT-2IT-1A3, *Cancer Biother.Radiopharm.*, 2001, **16**(6), 483–494.

70 B. Gutfilen, S. Souza and G. Valentini, Copper-64: a real theranostic agent, *Drug Des., Dev. Ther.*, 2018, **12**, 3235.

71 N. Smith, D. Bowers and D. Ehst, he production, separation, and use of ^{67}Cu for radioimmunotherapy: a review, *Appl. Radiat. Isot.*, 2012, **70**(10), 2377–2383.

72 P. Rowshanfarzad, M. Sabet, A. Reza Jalilian and M. Kamalidehghan, An overview of copper radionuclides and production of ^{61}Cu by proton irradiation of natZn at a medical cyclotron, *Appl. Radiat. Isot.*, 2006, **64**(12), 1563–1573.

73 P. Rajec, V. Csiba, M. Leporis, M. Štefečka, E. L. Pataky, M. Reich, *et al.*, Preparation and characterization of nickel targets for cyclotron production of ^{64}Cu, *J. Radioanal. Nucl. Chem.*, 2010, **286**(3), 665–670.

74 C. M. Jeffery, S. V. Smith, A. H. Asad, S. Chan and R. I. Price, Routine production of copper-64 using 11.7MeV protons, *AIP Conf. Proc.*, 2012, **1509**(1), 84–90.

75 M. A. Avila-Rodriguez, J. A. Nye and R. J. Nickles, Simultaneous production of high specific activity ^{64}Cu and ^{61}Co with 11.4 MeV protons on enriched ^{64}Ni nuclei, *Appl. Radiat. Isot.*, 2007, **65**(10), 1115–1120.

76 D. W. McCarthy, R. E. Shefer, R. E. Klinkowstien, L. A. Bass, W. H. Margeneau, C. S. Cutler, *et al.*, Efficient production of high specific activity ^{64}Cu using a biomedical cyclotron, *Nucl. Med. Biol.*, 1997, **24**(1), 35–43.

77 A. Obata, S. Kasamatsu, D. W. McCarthy, M. J. Welch, H. Saji, Y. Yonekura, *et al.*, Production of therapeutic quantities of ^{64}Cu using a 12 MeV cyclotron, *Nucl. Med. Biol.*, 2003, **30**(5), 535–539.

78 J. De Reuck, K. Paemeleire, P. Santens, K. Strijckmans and I. Lemahieu, Cobalt-55 positron emission tomography in symptomatic atherosclerotic carotid artery disease: Borderzone versus territorial infarcts, *Clin. Neurol. Neurosurg.*, 2004, **106**(2), 77–81.

79 J. De Reuck, P. Santens, J. Keppens, J. De Bleecker, K. Strijckmans, P. Goethals, *et al.*, Cobalt-55 positron emission tomography in recurrent ischaemic stroke, *Clin. Neurol. Neurosurg.*, 1999, **101**(1), 15–18.

80 H. Jansen, R. Dierckx, J. Hew, A. Paans, J. Minderhoud and J. Korf, Positron emission tomography in primary brain tumours using cobalt-55, *Nucl. Med. Commun.*, 1997, **18**(8), 734–740.

81 T. Mastren, B. Marquez, D. Sultan, E. Bollinger, P. Eisenbeis, T. Voller, *et al.*, Cyclotron production of high - Specific activity ^{55}Co and in vivo evaluation of the stability of ^{55}Co metal-chelate-peptide complexes, *Mol. Imag.*, 2015, **14**(10), 7290.

82 J. Garousi, K. Andersson, J. Dam, B. Olsen, B. Mitran, A. Orlova, *et al.*, The use of radiocobalt as a label improves imaging of EGFR using DOTA-conjugated Affibody molecule, *Sci. Rep.*, 2017, **7**(1), 1–10.

83 J. Dam, B. Olsen, C. Baun, P. Høilund-Carlsen and H. Thisgaard, Vivo Evaluation of a bombesin analogue labeled with Ga-68 and Co-55/57, *Mol. Imag. Biol.*, 2016, **18**(3), 368–376.

84 P. Goethals, A. Volkaert, C. Vandewielle, R. Dierckx and N. Lameire, ^{55}Co-EDTA for renal imaging using positron emission tomography (PET): a feasibility study, *Nucl. Med. Biol.*, 2000, **27**(1), 77–81.

85 B. Mitran, H. Thisgaard, U. Rosenström, J. Dam, M. Larhed, V. Tolmachev, *et al.*, High contrast PET imaging of GRPR expression in prostate cancer using cobalt-labeled bombesin antagonist RM26, *Contrast Media Mol. Imaging*, 2017, 1–10.

86 M. Al-abyad, M. N. H. Comsan and S. M. Qaim, Excitation functions of proton-induced reactions on with particular reference to the production of ^{57}Co, *Appl. Radiat. Isot.*, 2009, **67**(1), 122–128.

87 A. G. Wain and I. L. Jenkins, Functions for the bombardment, *J. Inorg. Nucl. Chem.*, 1970, **32**(1970), 1419–1425.

88 H. F. Valdovinos, R. Hernandez, S. Graves, P. A. Ellison, T. E. Barnhart, C. P. Theuer, *et al.*, Cyclotron production and radiochemical separation of ^{55}Co and ^{58m}Co from ^{54}Fe, ^{58}Ni and ^{57}Fe targets, *Appl. Radiat. Isot.*, 2017, **130**, 90–101.

89 H. F. Valdovinos, S. Graves, T. Barnhart and R. J. Nickles, ^{55}Co separation from proton irradiated metallic nickel, *AIP Conf. Proc.*, 2014, **1626**(1), 217–220.

90 P. Goethals, A. Volkaert, C. Vandewielle, R. Dierckx and N. Lameire, ^{55}Co-EDTA for renal imaging using positron emission tomography (PET): A feasibility study, *Nucl. Med. Biol.*, 2000, **27**(1), 77–81.

91 M. Daube and R. Nickles, Development of myocardial perfusion tracers for positron emission tomography, *Int. J. Nucl. Med. Biol.*, 1985, **12**(4), 303–314.

92 I. F. Chaple and S. E. Lapi, Production and Use of the First-Row Transition Metal PET Radionuclides ^{43,44}Sc, ^{52}Mn, and ^{45}Ti, *J. Nucl. Med.*, 2018, **59**(11), 1655–1659.

93 C. M. Lewis, S. A. Graves, R. Hernandez, H. F. Valdovinos, T. E. Barnhart, W. Cai, *et al.*, ^{52}Mn production for PET/MRI tracking of human stem cells expressing divalent metal transporter 1 (DMT1), *Theranostics*, 2015, **5**(3), 227–239.

94 S. A. Graves, R. Hernandez, J. Fonslet, C. G. England, H. F. Valdovinos, P. A. Ellison, *et al.*, Novel Preparation Methods of ^{52}Mn for ImmunoPET Imaging, *Physiol. Behav.*, 2015, **26**(10), 2118–2124.

95 A. L. Wooten, B. C. Lewis, R. Laforest, S. V. Smith and S. E. Lapi. Cyclotron Production and PET/MR Imaging of ^{52}Mn, in *Proceedings of the 15th International Workshop on Targetry and Target Chemistry*. 2014.

96 G. J. Topping, P. Schaffer, C. Hoehr, T. J. Ruth and V. Sossi, Manganese-52 positron emission tomography tracer characterization and initial results in phantoms and in vivo, *Med. Phys.*, 2013, **40**(4), 042502-2–042502-8.

97 J. Fonslet, S. Tietze, A. I. Jensen, S. A. Graves and G. W. Severin, Optimized procedures for manganese-52: Production, separation and radiolabeling, *Appl. Radiat. Isot.*, 2017, **121**, 38–43.

98 A. I. Jensen, G. W. Severin, A. E. Hansen, F. P. Fliedner, R. Eliasen, L. Parhamifar, *et al.*, Remote-loading of liposomes with manganese-52 and in vivo evaluation of the stabilities of ^{52}Mn-DOTA and ^{64}Cu-DOTA using radiolabelled liposomes and PET imaging, *J. Controlled Release*, 2018, **269**, 100–109.

99 S. Busse, J. Brockmann and F. Rösch, Radiochemical separation of no-carrier-added radioniobium from zirconium targets for application of ^{90}Nb-labelled compounds, *Radiochim. Acta*, 2002, **90**(7), 411–416.

100 V. Radchenko, S. Busse and F. Roesch, Desferrioxamine as an appropriate chelator for ^{90}Nb: Comparison of its complexation properties for M-Df-Octreotide (M=Nb, Fe, Ga, Zr), *Nucl. Med. Biol.*, 2014, **41**(9), 721–727.

101 V. Radchenko, D. V. Filosofov, O. K. Bochko, N. A. Lebedev, A. V. Rakhimov, H. Hauser, *et al.*, Separation of ^{90}Nb from zirconium target for application in immuno-pet, *Radiochim. Acta*, 2014, **102**(5), 433–442.

102 V. Radchenko, H. Hauser, M. Eisenhut, D. J. Vugts, G. A. Van Dongen and F. Roesch, ^{90}Nb - A potential PET nuclide: Production and labeling of monoclonal antibodies, *Radiochim. Acta*, 2012, **100**(11), 857–864.

103 V. Radchenko, D. V. Filosofov, J. Dadakhanov, D. V. Karaivanov, A. Marinova, A. Baimukhanova, *et al.*, Direct flow separation strategy, to isolate no-carrier-added ^{90}Nb from irradiated Mo or Zr targets, *Radiochim. Acta*, 2016, **104**(9), 625–634.

104 A. De La Fuente, V. Radchenko, T. Tsotakos, C. Tsoukalas, M. Paravatou-Petsotas, A. Harris, *et al.*, Conjugation, labelling and in vitro/in vivo assessment of an anti-VEGF monoclonal antibody labelled with niobium isotopes, *J. Radioanal. Nucl. Chem.*, 2018, **318**(3), 1991–1997.

105 S. Busse, F. Rösch and S. M. Qaim, Cross section data for the production of the positron emitting niobium isotope ^{90}Nb via the 90Zr(p,n)-reaction, *Radiochim. Acta*, 2002, **90**(1), 1–5.

106 E. Koumarianou, N. Loktionova, M. Fellner, F. Roesch, O. Thews, D. Pawlak, *et al.*, ^{44}Sc-DOTA-BN [2-14] NH2 in comparison to ^{68}Ga-DOTA-BN [2-14] NH2 in pre-clinical investigation. Is ^{44}Sc a potential radionuclide for PET?, *Appl. Radiat. Isot.*, 2012, **70**(12), 2669–2676.

107 H. Honarvar, C. Müller, S. Cohrs, S. Haller, K. Westerlund, A. Karlström, *et al.*, Evaluation of the first ^{44}Sc-labeled Affibody molecule for imaging of HER2-expressing tumors, *Nucl. Med. Biol.*, 2017, **45**, 15–21.

108 A. Khawar, E. Eppard, J. Sinnes, F. Roesch, H. Ahmadzadehfar, S. Kürpig, *et al.*, [^{44}Sc] Sc-PSMA-617 biodistribution and dosimetry in patients with metastatic castration-resistant prostate carcinoma, *Clin. Nucl. Med.*, 2018, **43**(5), 323–330.

109 G. Orteca, J. Sinnes, S. Rubagotti, M. Iori, P. Capponi, M. Piel, *et al.*, Gallium-68 and scandium-44 labelled radiotracers based on curcumin structure linked to bifunctional chelators: Synthesis and characterization of potential PET radiotracers, *J. Inorg. Biochem.*, 2020, **204**, 110954.

110 R. Hernandez, H. F. Valdovinos, Y. Yang, R. Chakravarty, H. Hong, T. E. Barnhart, *et al.*, ^{44}Sc: An attractive isotope for peptide-based PET imaging, *Mol. Pharm.*, 2014, **11**(8), 2954–2961.

111 E. Eppard, A. de la Fuente, M. Benešová, A. Khawar, R. A. Bundschuh, F. C. Gärtner, *et al.*, Clinical translation and first in-human use of [^{44}Sc]Sc-PSMA-617 for pet

imaging of metastasized castrate-resistant prostate cancer, *Theranostics*, 2017, **7**(18), 4359.

112 K. Siwowska, P. Guzik, K. Domnanich, J. Monné Rodríguez, P. Bernhardt, B. Ponsard, *et al.*, Therapeutic potential of ^{47}Sc in comparison to ^{177}Lu and ^{90}Y: Preclinical investigations, *Pharmaceutics*, 2019, **11**(8), 424.

113 V. Radchenko, C. A. Meyer, J. W. Engle, C. M. Naranjo, G. A. Unc, T. Mastren, *et al.*, Separation of ^{44}Ti from proton irradiated scandium by using solid-phase extraction chromatography and design of $^{44Ti/44}$Sc generator system, *J. Chromatogr. A*, 2016, **1477**, 39–46.

114 S. Krajewski, I. Cydzik, K. Abbas, A. Bulgheroni, F. Simonelli, U. Holzwarth, *et al.*, Cyclotron production of ^{44}Sc for clinical application, *Radiochim. Acta*, 2013, **101**(5), 333–338.

115 S. Banerjee, M. Pillai and N. Ramamoorthy, Evolution of Tc-99m in diagnostic radiopharmaceuticals, *Semin. Nucl. Med.*, 2001, **31**(4), 260–277.

116 H. Bigott, D. McCarthy, F. Wüst, J. Dahlheimer, D. R. Piwnica-Worms and M. Welch, Production, processing and uses of ^{94m}Tc. Journal of Labelled Compounds and Radiopharmaceuticals, *J. Labelled Compd. Radiopharm.*, 2001, **44**(S1), S119–S121.

117 C. Stone, B. Christian, R. Nickles and S. Perlman, Technetium 94m-labeled methoxyisobutyl isonitrile: dosimetry and resting cardiac imaging with positron emission tomography, *J. Nucl. Cardiol.*, 1994, **1**(5), 425–433.

118 H. Bigott, E. Parent, L. Luyt, J. Katzenellenbogen and M. Welch, Design and synthesis of functionalized cyclopentadienyl tricarbonylmetal complexes for technetium-94m PET imaging of estrogen receptors, *Bioconjugate Chem.*, 2005, **16**(2), 255–264.

119 C. D. Illan and B. W. Wieland, *Evaluation of a recoil-escape fiber target using 94Mo (p,n) 94mTc to produce 94TcO4-precursor for radiolabeled compounds useful in positron emission tomography*, Duke University Medical Center, Durham NC, 2001.

120 S. M. Qaim, Production of high purity ^{94m}Tc for positron emission tomography studies, *Nucl. Med. Biol.*, 2000, **27**(4), 323–328.

121 B. T. Christian, R. J. Nickles, C. K. Stone, T. L. Mulnix and J. Clark, Improving the radionuclidic purity of ^{94m}Tc for PET imaging, *Appl. Radiat. Isot.*, 1995, **46**(2), 69–73.

122 F. Rösch and S. M. Qaim, Nuclear Data Relevant to the Production of the Positron Emitting Technetium Isotope ^{94m}Tc via the ^{94}Mo(p,n)-reaction, *Radiochim. Acta*, 1993, **62**(3), 115–122.

123 X. Hou, J. Tanguay, K. Buckley, P. Schaffer, F. Bénard, T. J. Ruth, *et al.*, Molybdenum target specifications for cyclotron production of ^{99m}Tc based on patient dose estimates, *Phys. Med. Biol.*, 2015, **61**(2), 542–553.

124 M. Sadeghi, M. Enferadi and H. Nadi, ^{45}Ti, a candidate for positron emission tomography: Study of the cyclotron production, *Radiochemistry*, 2011, **53**(4), 411–414.

125 A. L. Vavere, R. Laforest and M. J. Welch, Production, processing and small animal PET imaging of titanium-45, *Nucl. Med. Biol.*, 2005, **32**(2), 117–122.

126 A. Vavere and M. Welch, Preparation, biodistribution, and small animal PET of ^{45}Ti-transferrin, *J. Nucl. Med.*, 2005, **46**(4), 683–690.

127 F. Chen, H. F. Valdovinos, R. Hernandez, S. Goel, T. E. Barnhart and W. Cai, Intrinsic radiolabeling of Titanium-45 using mesoporous silica nanoparticles, *Acta Pharmacol. Sin.*, 2017, **38**(6), 907–913.

128 S. Kuhn, I. Spahn, B. Scholten and H. H. Coenen, Positron and γ-ray intensities in the decay of ^{45}Ti, *Radiochim. Acta*, 2015, **103**(6), 403–409.

129 F. Rösch, S. Qaim and G. Stöcklin, Production of the positron emitting radioisotope ^{86}Y for nuclear medical application, *Appl. Radiat. Isot.*, 1993, **44**(4), 677–681.

130 T. K. Nayak, K. Garmestani, K. E. Baidoo, D. E. Milenic and M. W. Brechbiel, PET imaging of tumor angiogenesis in mice with VEGF-A-targeted ^{86}Y-CHX-A‴-DTPA-bevacizumab, *Int. J. Cancer*, 2011, **128**(4), 920–926.

131 T. Wadas, E. Wong, G. Weisman and C. Anderson, Coordinating radiometals of copper, gallium, indium, yttrium, and zirconium for PET and SPECT imaging of disease, *Chem. Rev.*, 2010, **110**(5), 2858–2902.

132 T. Clifford, C. Boswell, G. Biddlecombe, J. Lewis and M. Brechbiel, Validation of a Novel CHX-A ''Derivative Suitable for Peptide Conjugation: Small Animal PET/CT Imaging Using Yttrium-86-CHX-A ''-Octreotide, *J. Med. Chem.*, 2006, **49**(14), 4297–4304.

133 L. Wei, X. Zhang, F. Gallazzi, Y. Miao, X. Jin, M. Brechbiel, *et al.*, Melanoma imaging using ^{111}In-, ^{86}Y-and ^{68}Ga-labeled CHX-A ″-Re (Arg11) CCMSH, *Nucl. Med. Biol.*, 2009, **36**(4), 345–354.

134 H. Chong, K. Garmestani, D. Ma, D. Milenic, T. Overstreet and M. Brechbiel, Synthesis and Biological Evaluation of Novel Macrocyclic Ligands with Pendent Donor Groups as Potential Yttrium Chelators for Radioimmunotherapy with Improved Complex Formation Kinetics, *J. Med. Chem.*, 2002, **45**(46), 3458–3464.

135 C. Kang, X. Sun, F. Jia, H. Song, Y. Chen, M. Lewis, *et al.*, Synthesis and preclinical evaluation of bifunctional ligands for improved chelation chemistry of ^{90}Y and ^{177}Lu for targeted radioimmunotherapy, *Bioconjugate Chem.*, 2012, **23**(9), 1775–1782.

136 L. Koi, R. Bergmann, K. Brüchner, J. Pietzsch, H. Pietzsch, M. Krause, *et al.*, Radiolabeled anti-EGFR-antibody improves local tumor control after external beam radiotherapy and offers theragnostic potential, *Radiother. Oncol.*, 2014, **110**(2), 362–369.

137 T. Nayak, K. Garmestani, K. Baidoo, D. Milenic and M. Brechbiel, Preparation, biological evaluation, and pharmacokinetics of the human anti-HER1 monoclonal antibody panitumumab labeled with ^{86}Y for quantitative PET of carcinoma, *J. Nucl. Med.*, 2010, **51**(6), 942–950.

138 S. Walrand, R. Barone, S. Pauwels and F. Jamar, Experimental facts supporting a red marrow uptake due to radiometal transchelation in ^{90}Y-DOTATOC therapy and relationship to the decrease of platelet counts, *Eur. J. Nucl. Med. Mol. Imag.*, 2011, **38**(7), 1270–1280.

139 M. Le Fur, N. Rotile, C. Correcher, V. Clavijo Jordan, A. Ross, C. Catana, *et al.*, Yttrium-86 Is a Positron Emitting Surrogate of Gadolinium for Noninvasive Quantification of Whole-Body Distribution of Gadolinium-Based Contrast Agents, *Angew. Chem. Int. Ed.*, 2020, **59**(4), 1474–1478.

140 G. Reischl, F. Rösch and H. J. Machulla, Electrochemical separation and purification of yttrium-86, *Radiochim. Acta*, 2002, **90**(4), 225–228.

141 J. Yoo, L. Tang, T. A. Perkins, D. J. Rowland, R. Laforest, J. S. Lewis, *et al.*, Preparation of high specific activity ^{86}Y using a small biomedical cyclotron, *Nucl. Med. Biol.*, 2005, **32**(8), 891–897.

142 M. A. Avila-Rodriguez, J. A. Nye and R. A. Nickles, Production and separation of non-carrier-added ^{86}Y from enriched ^{86}Sr targets, *Appl. Radiat. Isot.*, 2008, **66**(1), 9–13.

143 T. R. DeGrado, M. K. Pandey, J. F. Byrne, H. P. Engelbrecht, H. Jiang, A. B. Packard, *et al.*, Preparation and preliminary evaluation of ^{63}Zn-zinc citrate as a novel PET imaging biomarker for zinc, *J. Nucl. Med.*, 2014, **55**(8), 1348–1354.

144 M. Rostampour, M. Aboudzadeh, M. Sadeghi and S. Hamidi, Theoretical assessment of production routes for ^{63}Zn by cyclotron, *J. Radioanal. Nucl. Chem.*, 2016, **309**(2), 677–684.

145 T. R. DeGrado, B. J. Kemp, M. K. Pandey, H. Jiang, T. M. Gunderson, L. R. Linscheid, *et al.*, First PET imaging studies with ^{63}Zn-zinc citrate in healthy human participants and patients with Alzheimer disease, *Mol. Imag.*, 2016, **15**, 1–10.

146 M. Rostampour, M. Sadeghi, M. Aboudzadeh, K. Yousefi and S. Hamidi, Investigation of the thermal performance of natCu target for ^{63}Zn production, *Appl. Radiat. Isot.*, 2018, **141**, 1–4.

147 T. DeGrado, B. Kemp, M. Pandey, H. Jiang, T. Gunderson, L. Linscheid, *et al.*, First PET imaging studies with ^{63}Zn-zinc citrate in healthy human participants and patients with Alzheimer disease, *Mol. Imag.*, 2016, **15**, 1536012116673793.

148 M. Rostampour, M. Sadeghi, M. Aboudzadeh, S. Hamidi, N. Soltani, F. B. Novin, *et al.*, Experimental study and simulation of ^{63}Zn production via proton induce reaction, *Appl. Radiat. Isot.*, 2018, **136**, 32–36.

149 S. Heskamp, R. Raavé, O. Boerman, M. Rijpkema, V. Goncalves and F. Denat, ^{89}Zr-immuno-positron emission tomography in oncology: state-of-the-art ^{89}Zr radiochemistry, *Bioconjugate Chem.*, 2017, **28**(9), 2211–2223.

150 T. H. Oude Munnink, M. E. A. Arjaans, H. Timmer-Bosscha, C. P. Schröder, J. W. Hesselink, S. R. Vedelaar, *et al.*, PET with the ^{89}Zr-labeled transforming growth factor-β antibody fresolimumab in tumor models, *J. Nucl. Med.*, 2011, **52**(12), 2001–2008.

151 W. B. Nagengast, E. G. De Vries, G. A. Hospers, N. H. Mulder, J. R. De Jong, H. Hollema, *et al.*, In vivo VEGF imaging with radiolabeled bevacizumab in a human ovarian tumor xenograft, *J. Nucl. Med.*, 2007, **48**(8), 1313–1319.

152 J. Yoon, B. Park, E. Ryu, Y. An and S. Lee, Current Perspectives on ^{89}Zr-PET Imaging, *Int. J. Mol. Sci.*, 2020, **21**(12), 4309.

153 N. Bhatt, D. Pandya and T. Wadas, Recent advances in zirconium-89 chelator development. Molecules, *Molecules*, 2018, **23**(3), 638.

154 J. Holland, Predicting the thermodynamic stability of zirconium radiotracers, *Inorg. Chem.*, 2020, **59**(3), 2070–2082.

155 A. M. Dabkowski, S. J. Paisey, M. Talboys and C. Marshall, Optimization of cyclotron production for radiometal of zirconium 89, *Acta Phys. Pol., A*, 2015, **127**(5), 1479–1482.

156 A. Kasbollah, P. Eu, S. Cowell and P. Deb, Review on production of ^{89}Zr in a medical cyclotron for PET radiopharmaceuticals, *J. Nucl. Med. Technol.*, 2013, **41**(1), 35–41.

157 M. J. O'Hara, N. J. Murray, J. C. Carter and S. S. Morrison, Optimized anion exchange column isolation of zirconium-89 (^{89}Zr) from yttrium cyclotron target: Method development and implementation on an automated fluidic platform, *J. Chromatogr. A*, 2018, **1545**, 48–58.

158 G. Severin, J. Engle, T. Barnhart and R. Nickles, ^{89}Zr Radiochemistry for Positron Emission Tomography, *Med. Chem.*, 2011, **7**(5), 389–394.

159 W. E. Meijs, J. D. M. Herscheid, H. J. Haisma, R. Wijbrandts, F. van Langevelde, P. J. Van Leuffen, *et al.*, Production of highly pure no-carrier added ^{89}Zr for the labelling of antibodies with a positron emitter, *Appl. Radiat. Isot.*, 1994, **45**(12), 1143–1147.

160 J. W. Engle, H. Hong, Y. Zhang, H. F. Valdovinos, D. V. Myklejord, T. E. Barnhart, *et al.*, Positron emission tomography imaging of tumor angiogenesis with a ^{66}Ga-labeled monoclonal antibody, *Mol. Pharm.*, 2012, **9**(5), 1441–1448.

161 Ö. Ugur, P. J. Kothari, R. D. Finn, P. Zanzonico, S. Ruan, I. Guenther, *et al.*, Ga-66 labeled somatostatin analogue DOTA-DPhe1-Tyr3-octreotide as a potential agent for positron emission tomography imaging and receptor mediated internal radiotherapy of somatostatin receptor positive tumors, *Nucl. Med. Biol.*, 2002, **29**(2), 147–157.

162 M. Khan, S. Khan, S. El-Refaie, Z. Win, D. Rubello and A. Al-Nahhas, Clinical indications for gallium-68 positron emission tomography imaging, *Eur. J. Surg. Oncol.*, 2009, **35**(6), 561–567.

163 M. Perera, N. Papa, M. Roberts, M. Williams, C. Udovicich, I. Vela, *et al.*, Gallium-68 prostate-specific membrane antigen positron emission tomography in advanced prostate cancer—updated diagnostic utility, sensitivity, specificity, and distribution of prostate-specific membrane antigen-avid lesions: a systematic review and meta-, *Eur. Urol.*, 2020, **77**(4), 403–417.

164 C. Kratochwil, P. Flechsig, T. Lindner, L. Abderrahim, A. Altmann, W. Mier, *et al.*, ^{68}Ga-FAPI PET/CT: tracer uptake in 28 different kinds of cancer, *J. Nucl. Med.*, 2019, **60**(6), 801–805.

165 F. Giesel, C. Kratochwil, T. Lindner, M. Marschalek, A. Loktev, W. Lehnert, *et al.*, ^{68}Ga-FAPI PET/CT:

biodistribution and preliminary dosimetry estimate of 2 DOTA-containing FAP-targeting agents in patients with various cancers, *J. Nucl. Med.*, 2019, **60**(3), 386–392.

166 U. Hennrich and M. Benešová, [68Ga] Ga-DOTA-TOC: The First FDA-Approved ^{68}Ga-Radiopharmaceutical for PET Imaging, *Pharmaceuticals*, 2020, **13**(3), 38.

167 M. R. Lewis, D. E. Reichert, R. Laforest, W. H. Margenau, R. E. Shefer, R. E. Klinkowstein, *et al.*, Production and purification of gallium-66 for preparation of tumor-targeting radiopharmaceuticals, *Nucl. Med. Biol.*, 2002, **29**(6), 701–706.

168 M. E. Rodnick, C. Sollert, D. Stark, M. Clark, A. Katsifis, B. G. Hockley, *et al.*, Cyclotron-Based Production of ^{68}Ga, [^{68}Ga]$GaCl_3$, and [^{68}Ga]Ga-PSMA-11 from a Liquid Target, *EJNMMI Radiopharm. Chem*, 2020, **5**(1), 1–18.

169 B. J. B. Nelson, J. Wilson, S. Richter, M. J. M. Duke, M. Wuest and F. Wuest, Taking cyclotron ^{68}Ga production to the next level: Expeditious solid target production of ^{68}Ga for preparation of radiotracers, *Nucl. Med. Biol.*, 2020, **80**, 24–31.

170 J. W. Engle, V. Lopez-Rodriguez, R. E. Gaspar-Carcamo, H. F. Valdovinos, M. Valle-Gonzalez, F. Trejo-Ballado, *et al.*, Very high specific activity $^{66/68}$Ga from zinc targets for PET, *Appl. Radiat. Isot.*, 2012, **70**(8), 1792–1796.

171 S. Zeisler, A. Limoges, J. Kumlin, J. Siikanen and C. Hoehr, Fused Zinc Target for the Production of Gallium Radioisotopes, *Instruments*, 2019, **3**(1), 10.

172 H. Thisgaard, J. Kumlin, N. Langkjær, J. Chua, B. Hook, M. Jensen, *et al.*, Multi-curie production of gallium-68 on a biomedical cyclotron and automated radiolabelling of PSMA-11 and DOTATATE, *EJNMMI Radiopharm. Chem*, 2021, **6**(1), 1–11.

173 J. Kumlin, J. H. Dam, C. J. Chua, S. Borjian, A. Kassaian, B. Hook, *et al.*, Multi-Curie Production of Gallium-68 on a Biomedical Cyclotron, *Eur. J. Nucl. Med. Mol. Imag.*, 2019, **46**(suppl. 1, 1, SI), S39.

174 M. Enferadi, M. Sadeghi and H. Nadi, 72As, a powerful positron emitter for immunoimaging and receptor mapping: Study of the cyclotron production, *Radiochemistry*, 2011, **53**(4), 407–410.

175 P. A. Ellison, F. Chen, T. E. Barnhart, R. J. Nickles, W. Cai and O. T. Dejesus, Production and isolation of ^{72}As from proton irradiation of enriched $^{72}GeO_2$ for the development of targeted PET/MRI agents, in: *Proceedings of the 15th International Workshop on Targetry and Target Chemistry*. 2015.

176 M. Jennewein, M. Lewis, D. Zhao, E. Tsyganov, N. Slavine, J. He, *et al.*, Vascular imaging of solid tumors in rats with a radioactive arsenic-labeled antibody that binds exposed phosphatidylserine, *Clin. Cancer Res.*, 2008, **14**(5), 1377–1385.

177 P. Ellison, F. Chen, S. Goel, T. Barnhart, R. Nickles, O. DeJesus, *et al.*, Intrinsic and stable conjugation of thiolated mesoporous silica nanoparticles with radioarsenic, *ACS Appl. Mater. Interfaces*, 2017, **9**(8), 6772–6781.

178 P. A. Ellison, T. E. Barnhart, F. Chen, H. Hong, Y. Zhang, C. P. Theuer, *et al.*, High Yield Production and Radiochemical Isolation of Isotopically Pure Arsenic-72 and Novel Radioarsenic Labeling Strategies for the Development of Theranostic Radiopharmaceuticals, *Bioconjugate Chem.*, 2016, **27**(1), 179–188.

179 A. DeGraffenreid, Y. Feng, D. Wycoff, R. Morrow, M. Phipps, C. Cutler, *et al.*, Dithiol aryl arsenic compounds as potential diagnostic and therapeutic radiopharmaceuticals, *Inorg. Chem.*, 2016, **55**(16), 8091–8098.

180 W. Ali. *Evaluation of Nuclear Reaction Cross Sections Relevant to the Production of Emerging Diagnostic Radioisotopes Fe-52 and As-72*. Government College University, Lahore, 2012.

181 I. Spahn, G. F. Steyn, F. M. Nortier, H. H. Coenen and S. M. Qaim, Excitation functions of natGe(p,xn)^{71,72,73,74}As reactions up to 100 MeV with a focus on the production of ^{72}As for medical and ^{73}As for environmental studies, *Appl. Radiat. Isot.*, 2007, **65**(9), 1057–1064.

182 Y. Li, S. F. Shen, J. H. Gu, S. H. Shi and J. Y. Liu, A study on the decay of ^{72}As, *Chin. Phys.*, 2005, **14**, 487–493.

183 R. Guin, S. K. Das and S. K. Saha, Separation of carrier-free arsenic from germanium, *J. Radioanal. Nucl. Chem.*, 1998, **227**(1–2), 181–183.